University College London

Department of Chemistry

Electrochemistry in the Gas Phase

by

Sean P. McCormack

Ph.D. 2003

ProQuest Number: U642827

All rights reserved

INFORMATION TO ALL USERS
The quality of this reproduction is dependent upon the quality of the copy submitted.

In the unlikely event that the author did not send a complete manuscript
and there are missing pages, these will be noted. Also, if material had to be removed,
a note will indicate the deletion.

ProQuest U642827

Published by ProQuest LLC(2016). Copyright of the Dissertation is held by the Author.

ProQuest LLC
789 East Eisenhower Parkway
P.O. Box 1346
Ann Arbor, MI 48106-1346

ABSTRACT

The aim of this project was to apply liquid phase electrochemical methodology to the gas phase. This was achieved by considering a flame, which is a weak plasma, as the electrolyte. All plasmas contain ions, electrons, excited species and neutral atoms and molecules. A dual burner was designed and built which had the capability to deliver two different gas streams to the burner head to produce one flame, with two discreet halves. Using the flame created with this burner as background electrolyte and aspirated solutions of metal salts added to the flame to alter the ion concentration; traditional two and three electrode electrochemistry experiments were applied to this system.

This report discusses gas phase electrochemistry where ions in the gas phase comprise the electrode compartments and complete the electrical circuit. This thesis presents firstly a review of the literature pertaining to ions in flames, which includes natural flame ions and the ions created when metal salts are added to a flame. Electrochemical cells are also introduced and ions in solution are compared to ions in the gaseous phase. Diffusion potentials in a gaseous electrolyte will be introduced and discussed and the first evidence for there existence presented. Another important discovery will also be introduced and discussed namely the first redox potential measurements for gas phase ions.

PREFACE

This thesis is based on research carried out at University College London from September 2000 – September 2002. I wish to thank my colleagues and the personal of the Department of Chemistry for the pleasant atmosphere. I would also like to thank the Engineering and Physical Sciences Research Council (EPSRC) and Angela and Tony Fish for financial support.

I would also like to thank Professor Richard Compton (Oxford University) for his help especially with the diffusion potential work and for his support through Electrochemistry Communications.

I would also like to thank Professor David Williams (U.C.L.) for his help with the redox potential work; I would not have made this discovery without his help.

Many thanks are also due to Professor Williams students, Camilla Forssten, Dimitra Georganopoulou, Hanna Rajantie and Ali Morshed, with whom I shared a lab and many ups and downs.

Last but not least I would like to thank my parents Frank and Rita and the rest of my family and friends for their support during my studies.

London, April 2003

Sean McCormack

CONTENTS

References

LIST OF FIGURES

LIST OF TABLES

LIST OF SYMBOLS

a_i,	activity
$a_{products}$	are the activities of the products
$a_{reactants}$	are the activities of the reactants
c	concentration
d	probe diameter
e	the elementary charge
e^-	an electron
e^{-*}	a hot electron
f	electrostatic force between the point charges
f	the gas flow rate
j	flux
k	Boltzmann constant
k_1	rate constant
ln	natural log
n	number of electrons
n_i	number of ions
n_e	number of electrons
p	pressure
q_1	point charge
r	inter charge separation
t	tims / s
u	mobility
x	cartesian co-ordinate
y	cartesian co-ordinate
z	cartesian co-ordinate
z	number of transferring electrons
A	capture area
D	diffusion coefficients

E	Measured cell potential
E^{θ}	Standard Electrode Potential
E_{cell}	cell potential
E_i	ionisation energy
F	The Faraday Constant
$\Delta G_{hydrayion}$,	free energy of hydration
$\Delta G_{ionisation}$	free energy of ionisation
$\Delta G_{solvation}$	free energy of solvation
$\Delta H_{Ionisation}$,	enthalpy of ionisation
$\Delta S_{Ionisation}$,	entropy of ionisation
I	current
M_i^{θ}	is the standard state
N_A	Avogadro constant
N_i	number of ions
N_o	number atoms
R	gas constant
T	temperature
V_P	plasma potential
V_F.	floating potential
ε	relative permittivity
ε_0	vacuum permittivity
$\varepsilon/\varepsilon_0$	dielectric constant
ϕ	electrical potential
ϕ_s	solution electrical potential
ϕ_m	metal electrode electrical potential
$\Delta\phi_{m/s}$	potential drop across the electrode/solution interface
$\Delta\Phi_{diffusion}$	junction or diffusion potential.
γ	activity coefficient
$\gamma_{\pm}$	mean ionic activity coefficient

λ_D	Debye length
λ_{fp}	free path length
μ	electrochemical potential
σ	collisional cross section

Aspirated Metal salt Thermal Spray Deposition (AMTSD)

Chemical Vapour Deposition (CVD)

Counter Electrode (CE)

Electrostatic Spray Assisted Vapour Deposition (ESAVD)

Flame Ionisation Detector (FID)

Ionisation Energy (IE)

Low Density Poly Ethylene (LDPE)

Personal Computer (PC)

Primary Reaction Zone (PRZ)

Reference Electrode (RE)

Secondary Reaction Zone (SRZ)

Volt-Ampere Characteristic (VAC)

Working Electrode (WE)

left hand side (LHS)

electro motive force (e.m.f)

right hand side (RHS)

round-bottomed flasks (RBF)

1.0   Introduction

The ultimate aim of this project was to apply liquid phase electrochemical methodology to the gas phase. This was achieved by considering a flame, which is a weak plasma, as an electrolyte. All plasmas contain ion and electrons[1]. In a flame the ions and electrons are created thermally in the primary reaction zone. A dual burner was designed and built which had the capability to deliver two different gas streams to the burner head to produce one flame, with two discreet halves. Using the flame created with this burner as background electrolyte and aspirated solutions of metal salts added to the flame to alter the ion concentration; traditional two and three electrode electrochemistry experiments were applied to this system.

The literature has references to "Electrochemistry in the gas phase"[2] and "Voltammetry in gas phase environments"[3]. These gas phase experiments however rely on droplets of liquids or vapours condensing from the gas phase onto an insulator between a microelectrode and a reference electrode in order to complete the electrical circuit. This report presents gas phase electrochemical measurements where thermally generated atomic or molecular ions in a gaseous electrolyte complete the electrical circuit. Other gas phase electrochemical measurements that utilise gas phase ions include the conductivity in flames experiments made by Goodings[4] and the plasma electrochemical growth processes where gaseous ions are deposited under electrochemical control onto ion conducting layers[5,6,7].

This thesis presents firstly a review of the literature pertaining to ions in flames, which includes natural flame ions and the ions created when metal salts are added to a flame. Electrochemical cells will also be introduced and ions in solution will be compared to ions in the gaseous phase. In chapter 2 the experimental set up and procedures used to perform the experiments will be described. Chapter 3 will describe how the conductivity in a flame changes with different parameters and the effect of inserting the electrode into the flame is discussed. Electrochemical diffusion potentials and electrochemical redox potentials of gas phase ions will be

introduced and discussed in Chapters 4 and 5. Finally in Chapter 6 there will be a summary of the project and conclusions are drawn.

1.1   Ions in flames

The existence of ions in the gas phase (a flame), which are thermally generated, has been well documented[8]. A flame can be considered as weak plasma containing ions, electrons, excited species and neutrals with varying concentrations depending on what fuel, oxidant and carrier gases are being used. The ratios of the gas mixtures is important in determining the degree of ionisation, i.e. the flame can be fuel rich (FR), [FUEL] > [OXIDANT], or fuel lean (FL), [FUEL] < [OXIDANT] or stoichiometric [FUEL] = [OXIDANT]. Whether the gases are premixed or allowed to diffuse into the reaction zone is also important, as premixed gases produce a more uniform flame.

The charge carriers created in a flame are mostly atomic and molecular cations and free electrons and these are produced in a variety of ionisation processes in the Primary Reaction Zone (PRZ) of the flame. The PRZ is the bright luminous region at the base of the flame, shown schematically in figure 1.1. The PRZ is typically 0.1 mm thick at atmospheric pressures extending up to 4 mm from the burner[9]. The PRZ's merge into the Secondary Reaction Zone (SRZ), an area of secondary luminosity, figure 1.1, which is approximately isothermal with laminar flow. The edges of the SRZ are in contact with the relatively static and lower temperature atmosphere, which surrounds the flame, and thus there is some turbulent mixing at the edges of the flame. The concentration of ions in atmospheric flames is generally small, with a maximum of 10^{12} ions cm^{-3} in hydrocarbon flames, and it is thought that these ions do not play a role in the chemistry of combustion[10]. Two flame systems have been used in this work $CH_4/O_2/N_2$ and $H_2/O_2/N_2$, the ionisation processes in these flames are discussed next.
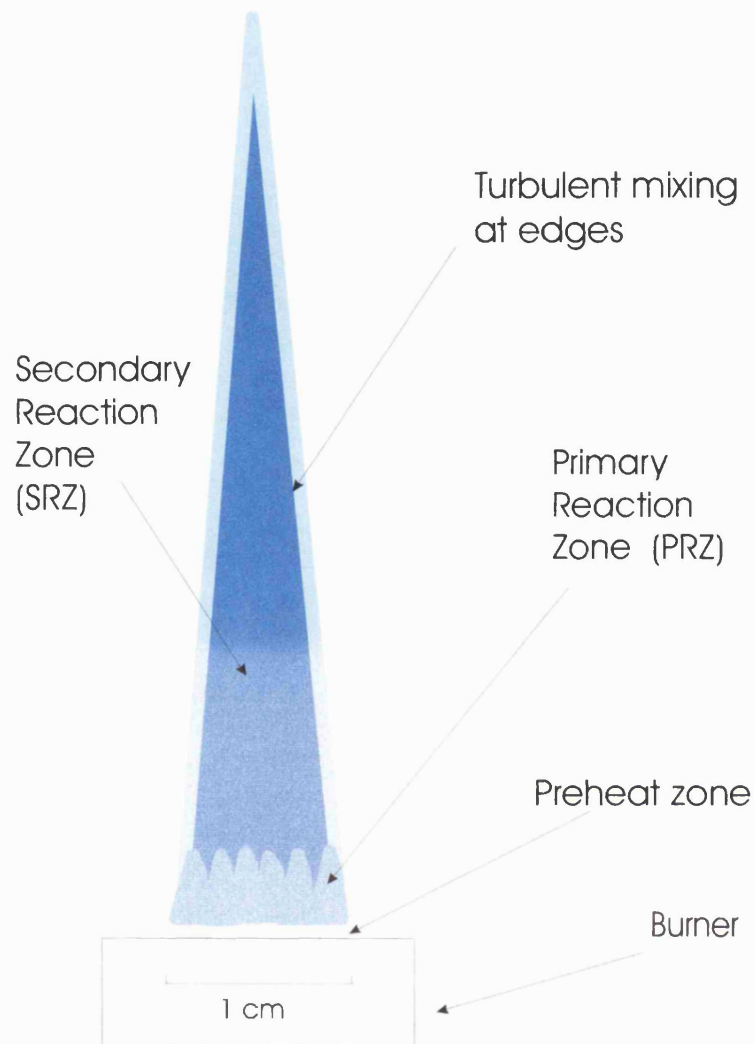
Figure 1.1 Schematic of a typical atmospheric flame produced from a Meker burner showing the Primary Reaction Zone and the Secondary Reaction Zone.

1.1.2 Ionisation in hydrocarbon flames

In a typical hydrocarbon/oxygen flame the maximum concentration of ions approaches 10^{12} ions cm^{-3}, out of a total of 10^{18} total species cm^{-3}, (which is about 1×10^{-6} mol fraction) at 2200 K. The concentration of ions peaks early in the burnt

gas region (SRZ) and decays downstream. The ions, which are predominantly CHO^+ and H_3O^+, in hydrocarbon flames, are created in the PRZ of the flame and are carried into the SRZ where they persist and can be measured. The principal techniques for determining the electron and ion concentrations in flames are: Microwave absorption[11], Mass Spectrometry[12,13] and Langmuir probes[14].

In a hydrocarbon (CH_4) flame the main ionisation reaction is thought to be a two-body chemi-ionisation reaction (1),

$$(1) \quad CH \quad + \quad O \quad \rightarrow \quad CHO^+ + \quad e^-$$

The rate constant for this reaction was measured[15] at 2200 K and found to be directly proportional to the product of the CH and O concentrations, and is, $k_1 = 1.7 \times 10^{-11}$ cm^3 molecule^{-1} s^{-1}.

The primary CHO^+ ion can then initiate a whole series of proton transfer reactions, examples of which are given in reactions (2)-(3), with flame intermediates of higher proton affinity to create different ions.

$$(2) \quad CHO^+ + \quad H_2O \quad \rightarrow \quad CO \quad + \quad H_3O^+$$

$$(3) \quad H_3O^+ + \quad M \quad \rightarrow \quad M^+ \quad + \quad H_2O \quad + \quad H$$

$$(4) \quad M^+ \quad + \quad e^- \quad + \quad A \quad \rightarrow \quad M \quad + \quad A$$
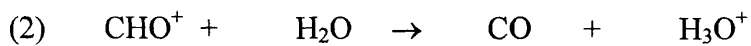
The ratio $[H_3O^+]/[CHO^+]$ is of the order $10^4 - 10^5$. As these ions are been generated at a constant rate and are decaying at a constant rate in a three-body recombination reaction (4), the concentration of ions at any point inside the SRZ of the flame is effectively constant (5).

$$(5) \qquad \frac{\delta[M^+]}{\delta t} = \frac{\delta[e^-]}{\delta t} = 0$$

The profile of total concentration of natural ions in a flame rises steadily through the PRZ of a flame where it peaks; there is then a steady decay in the SRZ [16],[17]. Some atoms and molecules form stable negative ions in the PRZ, of which O⁻ and O_2^- examples.[18] Usually the electron attachment energies are small, (1.41 and 0.42 kJ mol⁻¹ respectively in the above cases) so any negative ions react to form the neutral species and a free electron. In the SRZ of atmospheric flames however electrons are the main negatively charged species.

1.1.3 Ionisation in Hydrogen flames

The only charge carriers of any significance found in pure (without any additives) $H_2 + O_2 + N_2$ flames[19], are H_3O^+ and its hydrates (up to the tetrahydrate) and e⁻, with concentrations up to 10^9 ions cm⁻³. The following mechanisms of chemi-ionisation are suggested for fuel lean flames[20],[21], reactions (6) and (7),

$$(6) \qquad H + OH = H_2O^*$$

$$(7) \qquad H + H_2O^* \rightarrow H_3O^+ + e^-$$
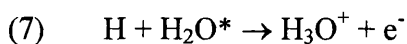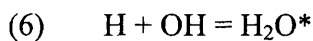
where * represents an excited electronic or vibrational state. For fuel rich flames[22], the following reactions are suggested, reactions (8) and (9),

$$(8) \qquad H + H = H_2^*$$

$$(9) \qquad H_2^* + OH \rightarrow H_3O^+ + e^-$$
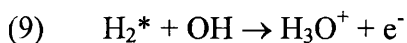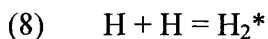
With the over all reaction being reaction (10),

(10) $H + H + OH \rightarrow H_3O^+ + e^-$
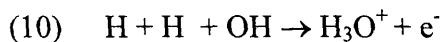
Nitrogen containing ions have also being assigned to some of the peaks of a mass spectra obtained from a flame of $H_2 + O_2 + N_2$. The peaks at mass 17, 18 and 30 amu are NH_3^+, NH_4^+ and NO^+ respectively and are responsible for between 0.01 % and 0.1 % of total ionisation, depending on the flame conditions. Experiments[23] in which argon was substituted for nitrogen as dilutent showed a decrease of the order 10^3 fold for these nitrogen-containing ions.

1.1.4 Ionisation of metals added to flames

The mechanisms responsible for the ionisation of metals in premixed flames of hydrogen (or of a hydrocarbon) with oxygen and nitrogen varies from metal to metal[24,25]: some experience thermal ionisation others either proton or charge transfer. Ionisation can also be caused by 'hot electrons' and by reactions with excited state species. The various ionisation mechanisms are discussed below and some examples given.

1.1.4.1 Thermal ionisation of metals added to flames

Thermal ionisation is more significant for metals with lower ionisation potentials. The reaction involved is the outcome of electronic excitation of, for example, an atom of a metal, A, in reaction (11).

(11) $A + M = A^* + M \rightarrow A^+ + e^- + M$
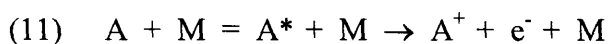
Where M is any molecule providing energy for the ionisation and A* is an excited state species. When an atom or molecule is introduced into a high (kinetic) energy environment, collisions with other species promote its outer electron to

progressively higher excited states and eventually the electron is separated from its mother (ion). The kinetics of thermal ionisation have been studied extensively for the alkali metals[26] and a general expression for the rate constant has been derived for the overall reaction (12),

(12) $A + M \rightarrow A^+ + e^- + M$
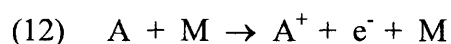
as $k_{12} = (9.9 \pm 2.7) \times 10^{-9} \, T^{1/2} \exp(-E_i/RT)$ molecule^{-1} cm^3 s^{-1}, where E_i is the ionisation energy of the metal, R is the gas constant and T is the measured flame temperature[27]. Although this expression for k_{12} is strictly only applicable to the alkali metals, it is expected to hold for other metals but with a different preexponential factor. Ions are lost by the reverse of reaction (12) which is a three body recombination involving a neutral species an ion and an electron. The rate constant for this reaction has the value $k_{-12} = 4.1 \pm 1.1 \times 10^{-24} \, T^{-1}$ cm^6 molecule^{-2} s^{-1} and is not dependant on flame composition or on which alkali metal is considered[28,29].

1.1.4.2 Ionisation of metals in flames by proton transfer

Another important mechanism for the production of metallic ions is proton transfer. This usually involves the natural and relatively abundant ion H_3O^+, (or CHO^+ in hydrocarbon flames) transferring a proton to some species with a greater proton affinity than H_2O. For metals, such species may be free atoms or molecules of an oxide or a hydroxide, thus generating ions in the reactions (13)-(15).

(13) $A + H_3O^+ \rightarrow A^+ + H_2O + H$

(14) $AO + H_3O^+ \rightarrow AOH^+ + H_2O$

(15) $AOH + H_3O^+ \rightarrow A^+ \cdot H_2O + H_2O$
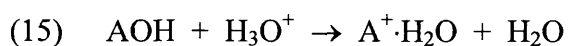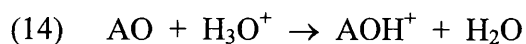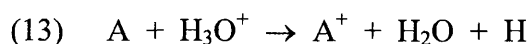
Reaction (13) here is a proton transfer reaction followed by rapid dissociation of AH^+ into A^+ and H. The products of reactions (13) – (15) are usually linked by equilibria such as reactions (16) and (17).

(16) $A^+ \cdot H_2O + M = A^+ + H_2O + M$

(17) $AOH^+ + H = A^+ + H_2O$
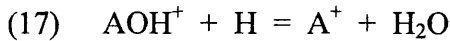
Which couple the concentrations of hydrated ions and the parent ion, and also of AOH^+ and A^+. These proton transfer reactions were studied by measuring the rate of change of concentration of H_3O^+, which is depleted in reactions (13) – (15) and the reverse of reaction (10)

The reversible reaction (10) governs the concentration of H_3O^+ in the burnt gases of simple flames of $H_2 + O_2 + N_2$.

The overall rate constant k_a for proton transfer was measured in flames of $H_2 + N_2 + O_2$ by Hayhurst and Telford[30] and was found to have the value $k_a = 10^{-9}$ ions cm^{-3} s^{-1}. This value is a mean of all the proton transfer reactions (13)-(15).

The ratio of the rates of thermal ionisation to proton transfer ionisation is $k_{12}[A][M]/k_a[A][H_3O^+]$, and substitution of typical values of rate constants and concentrations in the burnt gas of a flame (SRZ) indicates that thermal ionisation is faster than proton transfer ionisation. This is because the concentration of H_3O^+ is relatively low downstream in the SRZ of a flame, however close to the PRZ where the concentration of H_3O^+ is at its largest, the proton transfer reaction can dominate. An example of how these processes affect a particular species is given next.

When the transition metal copper, for example, is added to a flame, the reactions responsible for the production of some of the copper ion species according to Butler and Hayhurst are[31], reactions (18) and (19),

(18) $CuOH + H_3O^+ \rightarrow Cu^+ \cdot H_2O + H_2O$

(19) $Cu + H_3O^+ \rightarrow Cu^+ \cdot H_2O + H$
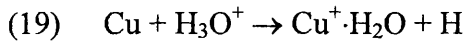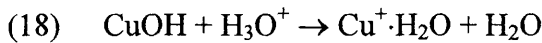
The rate constant for reaction (18) between an ion and a molecule with a large dipole moment is ca. 3.5×10^{-9} ions cm^{-3} s^{-1} at 2000 K and shows a negative temperature coefficient, with k_{18} varying as $T^{-2.0 \pm 1.0}$. The rate constant for the ion atom reaction (19) is smaller ca. 4×10^{-11} ions cm^{-3} s^{-1}, at 2000 K and shows a positive temperature coefficient i.e. at higher temperatures the activation energy for the reaction is lowered. The ionisation of copper has been investigated in both fuel rich and fuel lean flames and has led to the conclusion that the same ionisation mechanism operates in both fuel rich and fuel lean flames. Ionisation is faster in fuel lean flames however due to the greater abundance of CuHO, which is due to the greater abundance of OH as explained in section 1.1.3. This example goes to highlight some of the complications encountered when describing ionisation mechanisms in flames.

1.1.4.3 Ionisation of metals in flames by hot electrons

The third mechanism for ionisation in flames involves 'hot electrons' and is thought to be responsible for ionisation in the PRZ of flames containing hydrocarbons. The reaction is (20),

(20) $A + e^{-*} \rightarrow A^+ + 2e^-$
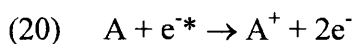
Where e^{-*} represents a hot electron. There is evidence[32] that free electrons can be hotter than the flame gases by 200 - 300 K in the reaction zone of a hydrocarbon flame. Ionisation by this method has not been studied thoroughly but is generally accepted as important overall.

1.1.4.4 Ionisation of metals in flames by excited state species

The final ionisation mechanism involves collisions between a metal atom and an electronically excited atom or molecule[33], e.g. H_2O^*, which is generated in the production of H_3O^+, reactions (6) and (7).

(6) $H + OH = H_2O^*$

(7) $H_2O^* + H = H_3O^+ + e^-$
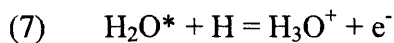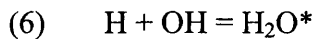
Collisions of H_2O^* with a flame species may either stabilise H_2O or cause dissociation to $H + OH$. However collisions with metals may result in the formation of ions through:

(21) $H_2O^* + A \rightarrow A^+.H_2O + e^-$
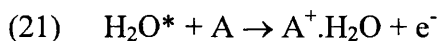
In fuel rich flames like the one used in this project the contribution from reaction (21) is always much less than for thermal ionisation, reaction (12). This is because the temperature in the SRZ of a fuel rich flame is higher than the temperature in the SRZ of a fuel lean one. Also, the flame radicals H and OH exceed their concentrations for final equilibrium to a greater extent in the reaction zone of a lean flame than in the reaction zone of a fuel rich flame, this results in a reduced production of H_2O^*.

1.1.5 Different metallic ion species created in a flame

As stated earlier the mechanism for the ionisation of metals in flames varies from metal to metal. The ionic species created and their percentage amount of total metallic ions also varies from metal to metal. The metallic ions that are created include mainly M^+, with lesser amounts of the molecular ions $M.H_2O^+$, $M(OH)H^+$, MH^+ etc. Generally the larger and more complex the molecular ion the less of it is created. For example when the transition metals nickel, copper, iron and cobalt are introduced into a flame with a burnt gas temperature of 2200 K the percentages of total metallic ions observed 1.25 mm above the burner are shown in table 1.

Table 1. Percentages of metallic ions observed in a hydrocarbon flame seeded with equimolar concentrations (0.25 M) of the metal chlorides measured by Mass Spectroscopy.[34]

Species	Ni	Cu	Fe	Co
M^+	77.2%	68.0 %	83.2%	77.2%
$M^+.H_2O$ $M(OH)H^+$	17.0%	23.0 %	9.6%	13.7%
$M^+.2H_2O$ $M(OH)H^+.H_2O$	2.0%	6.3 %	1.4%	1.5%
Other M species	3.8%	2.7 %	5.8%	7.6%

1.1.6 The absence of di- or tri- cations in atmospheric flames

No di- or tri- cations are formed at these flame temperatures, as the Second Ionisation Energy is to high, generally of the order of 2000 kJ mol^{-1}

1.1.7 The total concentration of ions in a flame

When an ionisable metal species is aspirated into a flame the total concentration of positive ions increases by an amount dependant on the concentration of the added solution. For the cases of potassium, which is ionised thermally and copper, which is ionised by proton transfer, both show similar trends. When a metal, M, is introduced into a flame the concentration of H_3O^+ is depleted by proton transfer to M and MOH as was shown in reactions (13) – (15). This in turn results in reaction (10) adjusting its equilibrium position to produce more H_3O^+ ions. The outcome is an increase in the total level of ionisation[35], see section 1.4.3 for a complete calculation of the concentration of ions in a flame.

1.2 Electrochemical cells

Electrochemical cells can vary widely in design and function but in general an electrochemical cell will consists of two or three electrodes – electron conductors, – in electrical contact with an electrolyte – an ionic conductor, which may be a liquid, a solid or in this case a gas. An electrode and its electrolyte comprise a half-cell, two half cells in series make an electrochemical cell. An electrochemical cell that produces electricity as a result of the spontaneous reaction occurring inside it is called a galvanic cell and an electrochemical cell in which a non-spontaneous reaction is driven by an external source of current is called an electrolytic cell.

1.2.1 The origins of electrode potentials

When an electrode is inserted into an electrolyte containing ions, it acts as a sink or source of electrons depending on the concentration and identity of the ions in the electrolyte, as in reaction (22)

$$(22) \quad M^+_{(electrolyte)} + e^-_{(electrode)} = M_{(electrolyte) \; or \; (electrode)}$$

After the transfer of an infatesimal amount of charge, the electrode's inner or Galvani potential will adopt a potential difference with respect to the solution's Galvani potential. When the forward and backward reactions at the electrode surface have reached equilibrium, with no net current flowing, the measured potential difference is the equilibrium potential difference, and we can say, equation (23),

$$(23) \quad \overline{\mu}_i^{Electrolyte} = \overline{\mu}_i^{Electrode}$$

where $\overline{\mu}_i^{Electrolyte}$ and $\overline{\mu}_i^{Electrode}$ are the electrochemical potential's of each species, i, in the electrolyte and electrode respectively for one electrode. Here the electrolyte can be a solid, liquid or gas.

In an aqueous electrolyte the electrode potential is related to the free energy of ionisation, $\Delta G_{ionisation}$ and the free energy of solvation, $\Delta G_{solvation}$ of the ionic speices dissolved in the aqueous solution surrounding the electrode surface, equation (24)

$$(24) \quad FE^{\theta} = \Delta G_{ionisation}^{\theta} + \Delta G_{solvation}^{\theta}$$

Electrode potentials in a plasma have also been described[36] and the conclusion is that the plasma behaves as an electrolyte and shows a characteristic potential drop at the metal plasma interface that is distinctive for every metal. This plasma electrode potential is related to the free energy of ionisation of the ionic species present in the gaseous environment surrounding the electrode surface. In an ideal plasma there would be no contribution to the electrode potential from the hydration of ions, equation (25)

$$(25) \quad FE^{\theta} = \Delta G_{ionisation}^{\theta}$$

1.2.2   Electrolytic cells

In an electrolytic cell a reaction can be made to happen at the electrode surface by applying a potential to, or polarising the electrode. An example of this is the Fe^{3+}/Fe^{2+} half-cell, where the composition of the solution can be controlled electrically, by shifting the equilibrium in reaction (26).

$$(26) \quad Fe^{3+} + e^- = Fe^{2+}$$
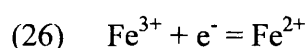
This is achieved by, for example, applying a suitable negative potential to an electrode immersed in a solution containing Fe^{3+} and Fe^{2+}. When the energy level (Fermi) of the electrons in the electrode exceed the energy levels of the highest unoccupied atomic orbitals in the Fe^{3+} ion they will transfer to the Fe^{3+} in solution, this will reduce Fe^{3+} to Fe^{2+} thus increasing the concentrations of Fe^{2+} and lowering the concentration of Fe^{3+}. The application of a positive potential to the same electrode will have the opposite effect.

1.2.3   Equilibrium electrochemistry

An electrochemical cell that has not reached chemical equilibrium can do electrical work as the reaction inside it drives electrons through an external circuit. The work that a given transfer of electrons can accomplish depends on the potential difference between the electrodes. The potential difference is called the cell potential and is measured in volts. A cell in which the reaction is at equilibrium can do no work, and the cell potential is zero. Therefore to make thermodynamic measurements on a cell by measuring the work it can do, we must ensure that it is operating reversibly, (not the case in cells with transference because the motion of the ions is not reversible). To do this we measure the cell potential when it is balanced by an opposing source of potential, the resulting potential difference is called the zero-current cell potential, E. The standard Gibbs free energy of the cell can then be calculated from equation (27),

(27) $\Delta G^{\theta} = - nFE^{\theta}$

where   n is the number of electrons and F is the Faraday constant and E^{θ} the standard cell potential. Equilibrium electrochemical measurements also enable other thermodynamic parameters to be obtained, such as entropies, enthalpies and equilibrium constants.

1.2.4 Voltaic cells

In a voltaic cell the potential difference that develops between the two electrodes can be measured. This is achieved by applying a voltage, which is equal and opposite to the voltage generated in the cell until such a point where no current is flowing. At this point if small changes in the applied voltage produce current flows in one direction or another, then we know the cell is working reversibly and the opposing voltage is equal to the maximum, which the cell can develop. Using one half of a cell as a reference half-cell, and the other half-cell as a variable half-cell, potential differences measure between different half-cells can then be compared versus the reference half-cell.

If ϕ_s is the solution (electrolyte) electrical potential and ϕ_m the metal electrode electrical potential, then the potential drop across the electrode/solution interface $\Delta\phi_{m/s}$ is given by equation (28),

(28) $\Delta\phi_{m/s} = \phi_m - \phi_s$

This quantity ($\Delta\phi_{m/s}$) has a fixed and precise value for any particular system. The absolute value of this quantity cannot be measured directly, however it can be compared to another (reference) half-cell, as in equation (29).

(29) $E_{CELL} = (\Delta\phi_{m/s})_{Variable} - (\Delta\phi_{m/s})_{Reference}$

1.2.5 The Nernst equation

Measured cell potentials, E are related to standard cell potentials, E^θ, and to the activity coefficients of the reagents in the cell reaction through the Nernst equation, equation (31). The activity, a_i, is a term introduced to allow for the nonideality of a solution and is equal to the product of the concentration, c and the mean ionic activity coefficient, $\gamma_\pm$, of the ions, i, as in equation (30).

$$(30) \qquad a_i = c\gamma_\pm = \frac{M_i}{M_i^\theta}\gamma_\pm$$

$$(31) \qquad E_{CELL} = E^\theta - \frac{RT}{nF}\ln\left(\frac{\Pi a_{products}}{\Pi a_{reac\,tan\,ts}}\right)$$

Where $a_{products}$ and $a_{reactants}$ are the activities of the products and reactants respectively and M_i^θ is the standard state.

1.2.6 Activities of gas phase ions

In electrolyte solutions the ion – ion interactions are strong and extend over a long range so electrolyte solutions can be regarded as ideal only at very low concentrations (below 10^{-3} mol L^{-1}) and any concentration above this level needs to be adjusted with the aid of an activity coefficient to get the effective concentration.

The activity coefficients, γ, of the ions in our gas phase system will approach unity because of the low concentration of these ions present ($10^{-6} - 10^{-7}$ mol fraction). Ions in solution tend to loose their unit activity when the concentration of the solution approaches 10^{-3} mol L^{-1}. This is equivalent to the ions being separated by a distance of 2.55 x 10^{-8} m. For the equivalent electrostatic interaction between gas phase ions the separation would need to be of the order 2.25 x 10^{-7} m, calculated using equation (32). This separation is equivalent to an ionic concentration of 8.76 x 10^{13} ions cm^{-3}. According to the literature (and the calculation in section 1.4.3) the

maximum ion concentration in atmospheric flames is approximately 10^{12} ions cm^{-3}, therefore the conclusion is that the ions in a flame are far enough apart so as not to affect each others activity.

$$(32) \quad f = \frac{q_1 q_2 /(4\pi\varepsilon)}{r^2} = \frac{q_1 q_2 /(4\pi\varepsilon_0)}{(\varepsilon/\varepsilon_0)r^2}$$

In equation (32), f is the electrostatic force between the point charges (ions), q_1 and q_2 are the two charges concerned, r the inter charge separation and ε and ε_0 are the relative and vacuum permittivity respectively. $\varepsilon/\varepsilon_0$ is known as the dielectric constant and it represents the effect of the medium in decreasing the force between the charges.

1.2.7 Junction potentials

When there is a junction between phases in the experimental set up, that has not been eliminated with the use of a salt bridge, another term needs to be added to the Nernst equation (31) to account for the reduction in the measured potential due to the diffusion of charge carriers across the electrolyte/electrolyte interface, this gives equation (33),

$$(33) \quad E_{CELL} = E^0 - \frac{RT}{nF}\ln\left(\frac{\Pi a_{products}}{\Pi a_{reac\tan ts}}\right) + \Delta\Phi_{diffusion}$$

where $\Delta\Phi_{diffusion}$ is the junction or diffusion potential.

For all the other junctions in an electrochemical cell there will also be junction potentials, (see figure 1.2) e.g. between the electrodes and connector clips. Keeping all the junctions in the experimental set up the same from experiment to experiment means we can neglect these contributions to the potential difference measurements. Which leaves us to consider the electrode/electrolyte potential drops and the

electrolyte/electrolyte potential drop that make up the cell potential, equation (34), which is equivalent to equation (33).
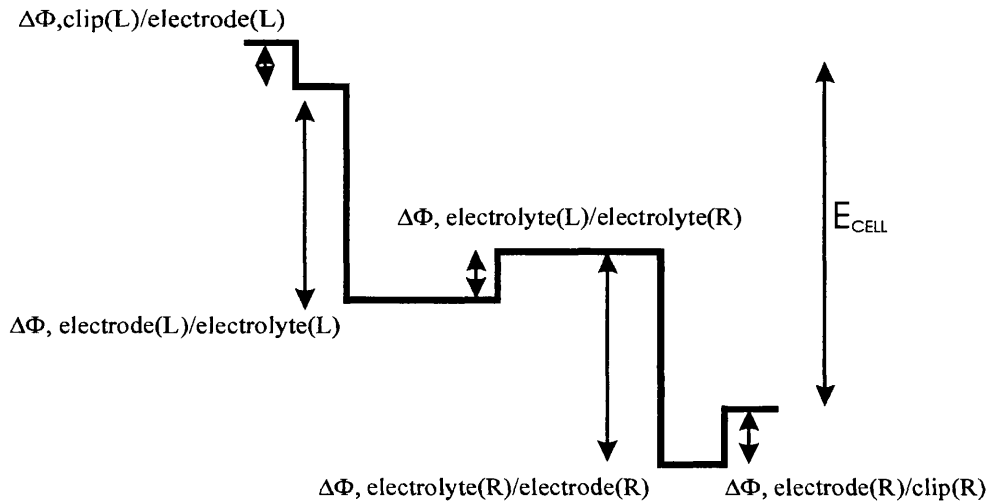
Figure 1.2. Shows the potential drop at all the junctions in a typical electrochemical cell.

(34) $E_{CELL} = (\Delta\Phi_{m/s})_{RHS} - (\Delta\Phi_{m/s})_{LHS} + \Delta\Phi_{diffusion}$

The origin of the diffusion potential may be understood by considering two HCl solutions of different concentrations c_1 and c_2 put into contact. Clearly there will be a large concentration gradient, $\delta[HCl]/\delta x$, at the interface between the two solutions. Such a concentration gradient will lead to diffusion of both H^+ and Cl^-, from high concentration to low concentration so as to tend to equalise the two concentrations.

The rate of diffusion is measured by the flux of the diffusing species. That is the number of moles passing through unit area in unit time. Thus at the interface we can write for the flux of protons (35),

$$(35) \qquad j_{H^+} = D_{H^+} \frac{\delta[H^+]}{\delta x}$$

and for the flux of the chloride ions (36),

$$(36) \qquad j_{Cl^-} = D_{Cl^-} \frac{\delta[Cl^-]}{\delta x}$$

where D_{H^+} and D_{Cl^-} are the diffusion coefficients of H^+ and Cl^- respectively. Figure 1.3 shows a schematic diagram of how the concentrations of ions and electrons might vary across a gas/gas interface with different concentrations on either side.

Initially shortly after the interface is formed, equation (37) is true,

$$(37) \qquad \frac{\delta[H^+]}{\delta x} = \frac{\delta[Cl^-]}{\delta x}$$

But we know that D_{H^+} is much larger than D_{Cl^-} because the protons are smaller and lighter and therefore more mobile than the chloride ions. It follows that initially the protons will diffuse at a faster rate than the chloride ions. As a result of this, a charge separation and hence a potential difference will be established across the interface between the two solutions. The solution with the lower concentration will become positively charged due to the gain in protons and the phase with higher concentration will become negatively charged due to excess anions. This will have the effect that the rate of the chloride ion transport will be accelerated (now that

migration will also contribute to the rate of mass transport) and the proton transport will be retarded. A steady state will eventually be reached, and at this steady state a potential difference will exist at the boundary of the two solutions, this is known as a liquid junction or diffusion potential. The magnitude of the diffusion potential can be estimated using the Henderson equation[37],(38),

$$
(38) \qquad \Delta\phi_{diffusion} = \left(\frac{u_+ - u_-}{u_+ + u_-} \right) \frac{RT}{F} \ln\left(\frac{\Sigma a_R}{\Sigma a_L} \right)
$$

where u_+ and u_- are the mobility's of the two charged species, (H^+ and Cl^- in this example) respectively. Thus the magnitude of the diffusion potential is dependant on the difference in the mobility's of the two charge carriers. Diffusion potentials also depend on the ratio a_R / a_L; if the two concentrations are equal the diffusion potential is predicted to disappear as would be anticipated.

The above model will also be applicable to the gas phase where there is a difference in mobility's between the two charge carriers and is discussed further in chapter 4. A schematic diagram of the charge separation between the two gases is shown in figure 1.3. Here the charge carriers are molecular or atomic cations and free electrons.
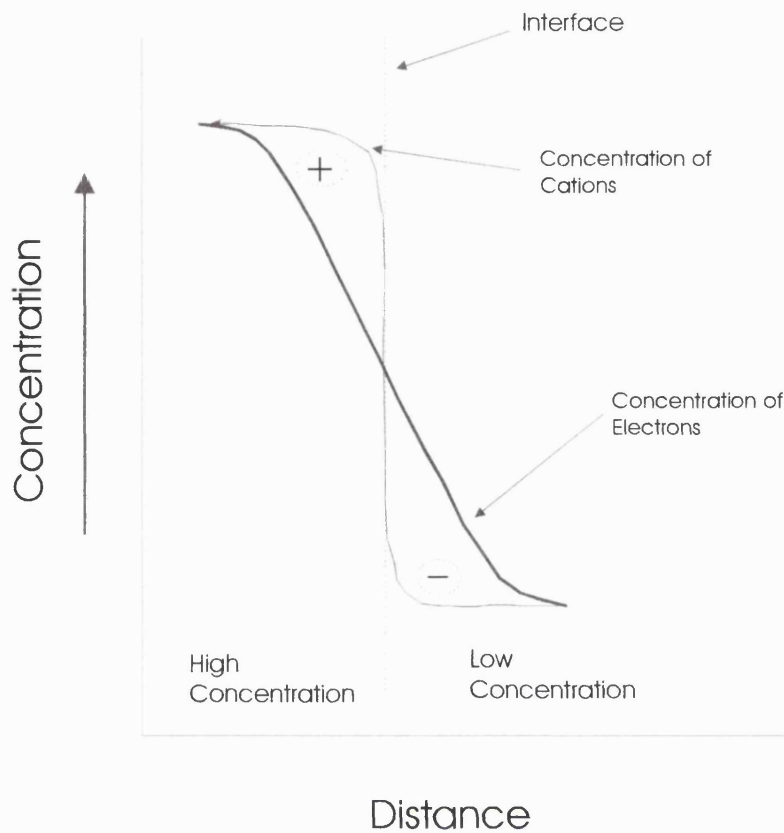
Figure 1.3 A schematic diagram of the differences in the rate of diffusion of cations and electrons across a gas/gas interface, from high to low concentrations.

1.3   Similarities between ions in the gaseous and liquid phases

In the liquid phase ions can exist dissolved in a solution. Similarly in the gaseous phase ions can exist, where the gas is a flame. In a liquid electrolyte the ions are stabilised by electrostatic forces and polarisation, whereas in a flame the ions are generated thermally and are relatively unstable. Coulomb forces acting between charged particles ensure a gas phase (flame) cation is, on average, surrounded by more than one electron[38],[39] this surrounding electron cloud provides an effective shielding of the positive ion charge. This situation is analogous to the liquid phase where an ion atmosphere surrounds an ion with charges opposite to that of the central ion.

1.3.1 Similarities between the solid/liquid and solid/gas interface's

Electrodes can be inserted into both media (liquid and gas) for the purpose of taking electrochemical measurements. In both cases (solid-gas, solid-liquid) the potential drop at the interface is similar, for polarised electrodes, figures 1.4 and 1.5 show schematic diagrams of the potential drop across the two interfaces. Both profiles show an exponential decay of potential away from the electrode surface, the only major difference being the length scale of the diffuse layer in the solution and the sheath layer in the gas phase.
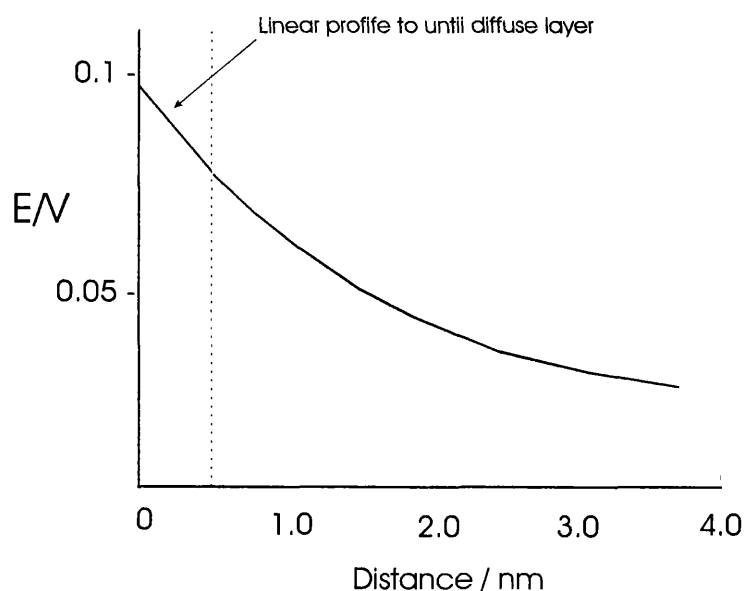
Figure 1.4 Schematic diagram of the potential profile through the solution side at a metal/solution interface, according to the Gouy-Chapman-Stern model. For a 10^{-2} M 1:1 electrolyte in water at 25 ^{0}C[40] and a potential difference of 100 mV.

The Debye layer is approximately 200 μm thick when the concentration of ions is approximately 10^{10} ions cm^{-3}, whereas the diffuse layer in the Gouy-Chapman-Stern model is approximately 5-6 nm when the concentration is 10^{-2} M (10^{19} ions cm^{-3}). The longer distance of the Debye length is due to the lower concentration of charge

carriers in the vicinity of that electrode. The lower concentration means that the electric field emanating from the electrode needs to protrude further into the bulk electrolyte to counter the charge.
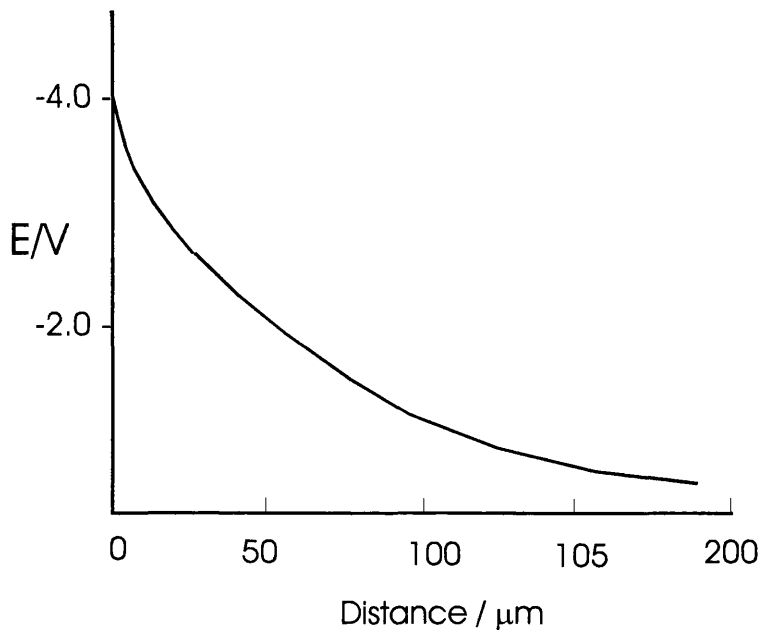
Figure 1.5 Schematic diagram of the potential profile through the plasma side of a metal/plasma interface. For a flame with an ion concentration of 10^{10} ions cm^{-3}.

1.3.2 Differences between a flame plasma and a liquid electrolyte

The obvious major differences (see table 2) between the two media are the temperatures, the densities and the mobility's of the constituents. Also the solvent effects are absent from the gas phase too. In solution an ions free energy may be calculated from the sum of its free energy of ionisation, $\Delta G_{ionisation}$ and its free energy of hydration $\Delta G_{hydrayion}$, whereas a gas phase ion has no contribution to its total free energy from the hydration of the ion. Overall a flame like a solution is electrically neutral, but statistically near any ion there is an excess of counter species, species of opposite charge. Thus the chemical potential, of any given

central ion, be it in the gas phase or solution phase, is lowered as a result of its columbic interactions with its oppositely charged atmosphere[41].

Table 2. Comparison of some of the physical properties of a standard cell (aqueous) and a gas phase cell (gas at 1800 K).

	GAS	WATER	Reference
density / g cm^{-3}	2.2×10^{-6}	1.0	42
mobility's[43]; cations electrons /cm^2 s^{-1} V^{-1}	5 4000	5.0×10^{-4}	41
diffusion coefficient[44] D / cm^2 s^{-1}	0.1 (273 K)	1×10^{-5}	42
dielectric constant[45]	1.0 (0° C)	78 (20° C)	43

1.3.3 Advantages of electrochemistry in the gas phase

Gas phase electrochemistry offers many benefits to the electrochemist. As well as the rapid mass transport (up to 50 m s^{-1}) observed in this environment, there is also approximately a five orders of magnitude increase in diffusion coefficients compared to the liquid phase. Gas phase electrochemistry also allows us to look through a potential window not available in solution electrochemistry, because of the absence of a solvent.

1.4 Conductivity in a flame

Electric probes can be used to determine the concentration of positive ions and electrons in a flame and were used as far back as 1906[46]. The most widely used is the probe developed by Langmuir[47] in 1924, now called the Langmuir probe, which is very simple in design but complex in theory. A schematic of a Langmuir probe is shown in figure 1.6. For flame investigation, metal wire probes of simple geometric shape, cylindrical or spherical, are mainly used. Metal wire probes are generally used because of their high melting points and ready availability. Depending on the flame type and necessary spatial resolution, a length of cylindrical probe may vary from more than one centimetre to several millimetres and in diameter from about a millimetre to several hundredths of a millimetre.
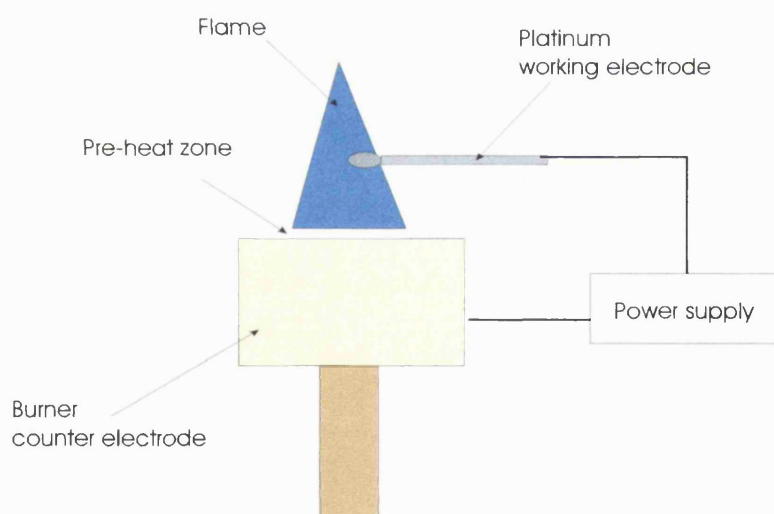
Figure 1.6 Schematic of the Langmuir probe set-up to make conductivity measurements in a flame.

The absolute values of the electric current through the probe as well as the thermoconductivity are dependent on the surface area of the probe. The probe material should be resistant to conditions in the flame and must not catalyse

reactions in the flame. For the experiments in this work platinum wire 1.0 mm diameter, which showed no visible fouling when inserted into the flame was used unless otherwise stated.

1.4.1   The volt-ampere characteristic

By varying the potential difference between the probe and the base electrode, it is possible to obtain a diagram of the current-to-probe dependence on its voltage, as shown in figure 1.7, from which flame characteristics of interest such as the concentration of charged species, can then be determined. This is the basis for the Flame Ionisation Detector (FID). The experimental part of this experiment is very
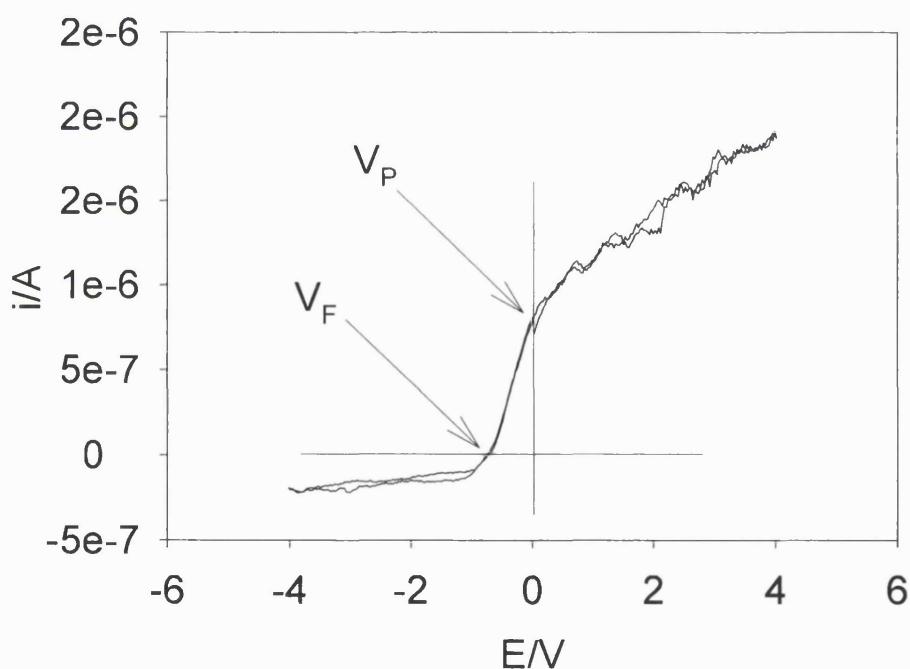
Figure 1.7 The volt-ampere characteristic obtained in a $H_2/O_2/N_2$ (1.6:0.6:1.0, L min^{-1}) flame with no additives, obtained using a 1.0 mm platinum wire probe placed 5.0 mm above the burner plate with ca. 2mm of electrode penetrating the flame and using the burner as counter electrode. Indicated on the plot are the plasma potential, V_P, and the floating potential, V_F.

simple, and it is not too difficult to obtain the Volt-Ampere Characteristic (VAC) curve. But the calculation of charged species concentrations presents some problems, because the theoretical model must describe the movement of charged species in the electric field in the vicinity of the probe, as well as in the undisturbed ambient plasma, in order to connect the charged species concentration with the current-to-probe at a certain probe voltage.

The shape of the VAC can be explained in the following way. When the probe has a high positive potential, it attracts electrons and repels positive ions. A space with an excess of negative charge forms around the probe; the volume of the space (sheath) surrounding the probe is dependant on the applied potential and the concentration of charge carriers in the flame. In this case (positive potential) only electron current flows to the probe. By reducing the positive potential of the probe, the sheath volume will be reduced, respectively. When the probe potential equals the potential of the surrounding plasma, the plasma potential, V_P in figure 1.7, the sheath will disappear. Now the probe does not influence the movement of the charged species and they come into contact with the surface of the probe as a result of convection only. As the velocities of electrons are much higher than those of positive ions, the current to the probe at V_P is mainly due to electrons. When the probe potential is biased negatively, electrons are repelled from it, and positive ions are attracted. The point where the electron and ion currents become equal is termed the floating potential V_f. The value of this floating potential is sensitive to the combustion conditions (see chapter 3).

1.4.2   The effect on the VAC of introducing metal ions into a flame

On the introduction of metal vapours to the flame, we generally see an increase in the ion current and an increase in the electron current as can be seen in figure 1.8, where a VAC obtained in a natural flame in compared to a VAC obtained in a flame seeded with 1.0 mM CsCl. The increase in currents is due to the low Ionisation

Energies (IE) of the metal ceasium (IE 376 kJ mol^{-1}), compared to the natural flame species[48], e.g. H and O_2 who's IE's are ca. 1300 kJ mol^{-1}. As expected a species with a lower IE will ionise to a greater extent than a species with a higher IE for a given amount of energy. As the flame retains its electroneutrality, the number of ions (n_i) produced must equal the number of electrons (n_e) produced, $(n_i) = (n_e)$, or more correctly the number of positive charges must equal the number of negative charges. The ionisation mechanism is dependant on which metals are used but in general involve, electron impact, collisional, chemi- and charge transfer reactions[49]. Figure 1.8 shows a VAC obtained in a natural unseeded flame and a VAC obtained in a flame seeded with a 1.0 mM CsCl solution. The increase in both the cation and electron currents are visible in the VAC of the seeded flame. The extra cations are Cs^+ and other cesium containing ions and the extra electrons are the other product of the ionisation process, $Cs \rightarrow Cs^+ + e^-$
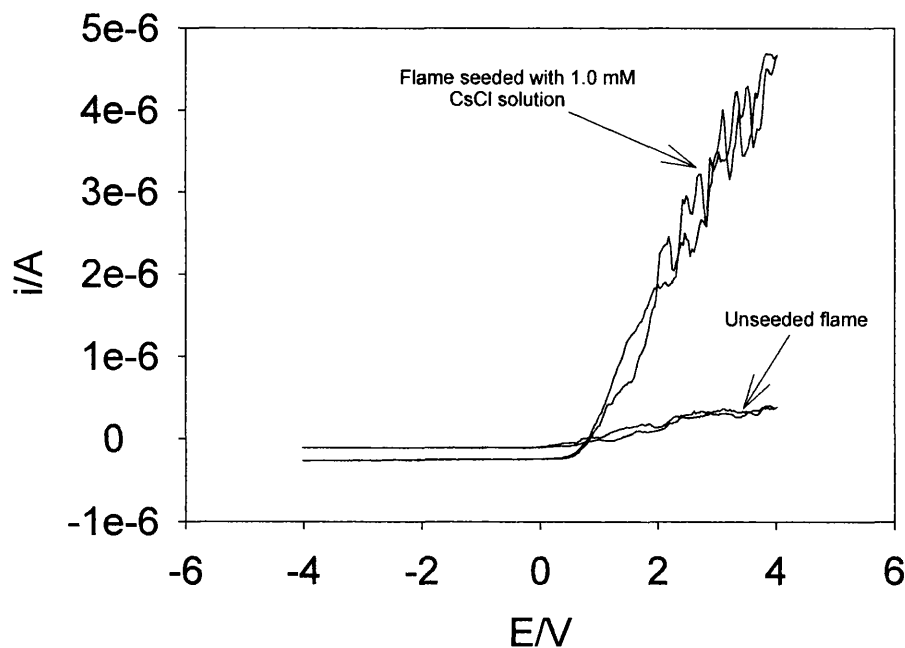
Figure 1.8 The increase in ion and electron currents on the introduction of a 1.0 mM solution of CsCl into a $H_2/O_2/N_2$ (1.6:0.6:1.0, L min^{-1}) flame, obtained using a 1.0 mm platinum wire probe placed 5.0 mm above the burner plate, with ca. 2 mm of electrode penetrating the flame and using the burner as counter electrode.

The increase in currents generated at a particular voltage is directly proportional to the concentration of metal salt aspirated in to the flame gases. This can be seen in figure 3.7 chapter 3, where the concentration of KCl aspirated into the flame gases is plotted against the currents generated in the flame with a probe biased at − 3V, here the relationship is linear, with the straight line on the plot being a least squares fit. Outside the range of concentrations 1.0 mM − 1.0 μM the relationship deviates from linearity. At higher concentrations, above the milimolar range there is too much metal salt going into the flame and the proportion of it that is ionised falls as a consequence. At lower concentrations the purity of water, the cleanliness of the glassware and the dilution technique used to dilute the solutions, all introduced a margin of error.

1.4.3   Calculation of the concentration of ions in a flame

To calculate absolute values of positive ion or electron concentrations in flames, using a Langmuir type probe it is necessary to determine the conditions of movement of charged species through the (sheath) layer boundary and inside the layer surrounding the probe. This, "mode of operation" of the probe depends on the ratio of the free path length (λ_{fp}) of the ions, the width of the sheath of volume charge (λ_D) and the probe diameter (d). For example in a collisionless ($\lambda_{fp}/\lambda_D \gg 1$), thin ($\lambda_D/d \ll 1$) sheath of volume charge, at electron saturation current, all electrons coming through the layer boundary enter the probe and the current is giving by equation (39).

However in the experimental set-up used in this report where the probe diameter was 1.0 mm and the experiments performed at atmospheric pressure. The mode of operation was, $d > \lambda_D > \lambda_{fp}$, i.e. the charged species collide inside the layer of volume charge and the layer is thin compared to the probe size. This experimental set-up is said to be operating in the mode of the collisional thin sheath. In such cases the current to the probe cannot be found as easily.

An estimation of the ion concentration can still be made if we consider the mean free path in a flame at atmospheric pressure is very small ca 10^{-4} cm and convection is fast, 28 m s^{-1} in this work, (see the flame properties in the experimental section), so the transport of ions into the capture area will be dominated by the convective flow.

Using equation (39) the current to a cylindrical probe will be given by

(39) $I = jeA$

Where j is the flux of ions into the capture area, e is the elementary charge and A the capture area. j can be calculated from, (40),

(40) $j = n_i f$

where n_i is the number density of ions and f is the gas flow rate. The capture area, A is the area where any ions passing through this area are captured by the electrode (see figure 1.9) and is calculated by, (41),

(41) $A = (d + 2 \lambda_D)(1 + \lambda_D)$

The sheath thickness, λ_D is given by the equation[50],(42),

(42) $\lambda_D = (kT/4\pi ne^2)^{0.5} \approx 69.1(T/n)^{0.5}$

where T is expressed in degrees Kelvin and n is the ion concentration.

The values of some of the parameters involved with this experimental set-up have been calculated using the data from figure 1.8. These include the sheath thickness (λ_D), the free path length (λ_{fp}) and the concentration of cations for a natural $H_2/O_2/N_2$ flame and a $H_2/O_2/N_2$ flame seeded with a 0.1 mM CsCl solution. The

results are presented in the table 2. The mean free paths (λ_{fp}) in table 3 were calculated[51] from equation (43).

$$(43) \quad \lambda_{fp} = \frac{RT}{\sqrt{2}N_A \sigma p}$$

where N_A is Avogadro constant, σ the collisional cross sections and p the pressure.
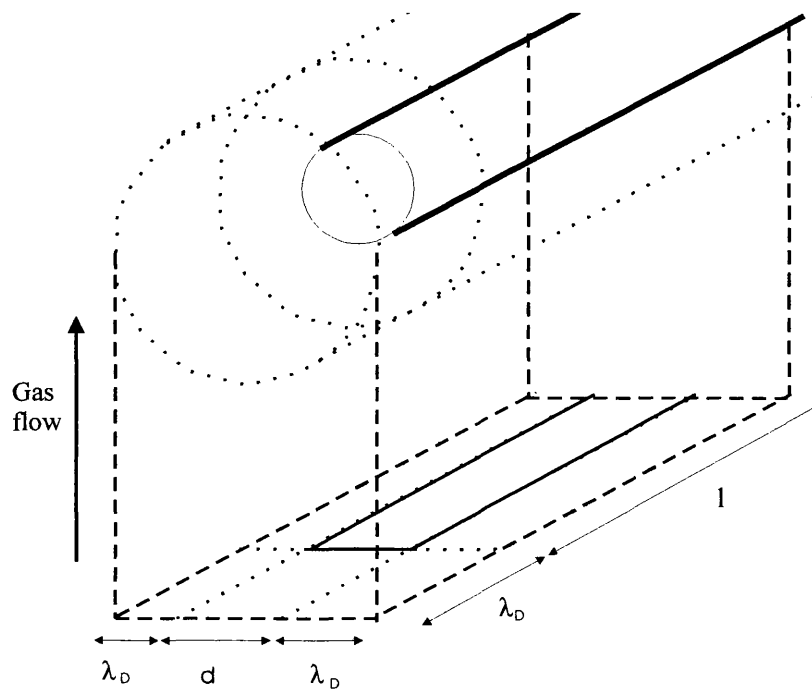
Figure 1.9 A schematic diagram of the capture area developed by a biased probe in a flowing flame.

Table 3. An estimation of the values of some of the parameters associated with the experimental set up used in this work. Calculated from the data in figure1. 8.

	$H_2/O_2/N_2$ Flame unseeded	$H_2/O_2/N_2$ Flame seeded with 1.0 mM CsCl
d Probe diameter / cm	0.1	0.1
l Probe length / cm	0.2	0.2
λ_D (sheath thickness) / cm	0.06	0.0364
A Capture area cm^2	0.0572	0.0408
n_i concentration of cations / cm^{-3}	4.14×10^9	1.43×10^{10}
f gas flow rate cm s^{-1}	2800	2800
λ_{fp} (Free path length) / cm	5.3×10^{-4} (H_3O^+)	3.8×10^{-5} (Cs^+)

The interesting thing to note in the data presented in table.3 is the reduction in the sheath thickness, λ_D and thus the reduction in the capture area as the concentration of ions increases. This can be understood by considering the electric field radiating from the electrode. This electric field is neutralised by a surrounding sheath of oppositely charged species from the electrolyte. The electric field does not need to penetrate as far into the electrolyte when the concentration of charge carriers in the electrolyte is higher and so the sheath thickness does not need to be as long. Also in the data presented in table 3 for this experimental set up, it can be seen that the sheath thickness (the charged area surrounding the electrode) is greater than the free path length of the ions in this system. This means that ions entering the capture area

do not necessarily come into contact with the electrode surface but may in fact collide inside the sheath resulting in the neutralisation of the ion or indeed the creation of new ionic species. The data in table 3 is only representative for a cation sheath at negative potentials, the sheath thickness at positive potentials will be different.

1.5 Deposition of metal species from the gas phase

There are several methods of depositing metal species from the gas phase. Some of the methods have similarities with processes encountered in this project and will be discussed below.

1.5.1 The combustion torch

In the combustion torch method coatings are sprayed from rod or wire stock or from powder material. The material is fed into a flame that melts it. The molten stock then is stripped from the end of the wire and atomised by a high-velocity stream of compressed air or other gases, coating the materials onto the work piece. Depending on the substrate, bonding occurs because of mechanical interlock with a roughened surface and/or because of Van der Waals forces (i.e., mutual attraction and cohesion between two surfaces).

1.5.2 Plasma spray deposition

Plasma spraying involves the introduction of a flow of gas (usually argon-based) between a water-cooled copper anode and a tungsten cathode. A direct current arc passes through the gases and ionises it to form a plasma. The plasma heats the powder coating to a molten state. Compressed gas propels the material to the work piece at high speeds.

1.5.3 Physical vapour deposition

This section will be split into two parts, Ion plating and Ion implantation.

1.5.3.1 Ion Plating/Plasma-Based

Plasma-based plating is the most common form of ion plating. In plasma-based plating, the substrate is placed in close proximity to a plasma. Ions are then accelerated from the plasma by a negative bias onto the substrate. The accelerated ions in the plasma deposit the coating on the surface substrate with a spectrum of energies.

1.5.3.2 Ion Implantation

Ion implantation does not produce a discrete coating; rather, the process alters the elemental chemical composition of the surface of the substrate by forming an alloy with energetic ions. A beam of charged ions of the desired element is formed by feeding a gas into the ion source where electrons, emitted from a hot filament, ionise the gas and form a plasma. An electrically biased extraction electrode focuses the ions into a beam. If the energy is high enough, ions alloy with the substrate instead of onto the surface, changing the surface composition.

The processes outlined here in section 1.5 can be used to describe the processes we see occurring when an electrode is inserted into a flame seeded with metal species. This will be discussed further in the results section, chapter 3.

1.6 Summary of introduction

The existence of ions in the gaseous phase has been well documented. A gaseous cloud in which ions exist is called plasma. A flame is a weak plasma because the

concentration of ions is low ca. 10^{12} cm^{-3}. These gaseous ions are similar to liquid phase ions and can be compared to them. The similarities include;

- Both ions (liquid and gas) exist in dynamic media
- The Debye-Hückle atmospheres that surrounds the ions consist of oppositely charged species
- The potential drop through the atmospheres is similar.

A flame was chosen for this project because of the low set up cost and a flame can be considered as a wall-less reactor into which electrodes could be inserted. The other alternative, strong plasma needs containment and has higher capital costs. Using two flames in intimate contact with each other and standard electrochemical instruments, potentiostat and voltmeter, electrodes can be inserted into the flames and measurements taken, both potentiometric and amperometric.

An enormous amount of work has been done in this field and applications found for the technologies discovered. These include flame spraying, plasma deposition[52] and conductivity measurements (Flame Ionisation Detector). This project aims to fill some of the gaps in knowledge, experimental and theoretically, between plasma chemistry, physics and electrochemistry

2.0   Experimental

The experimental work in this project involved the design and construction of a new gas phase electrochemical cell. This gas phase electrochemical was a duel flow burner capable of creating two individual flames in intimate contact with each other. Platinum wire was used for the electrodes and standard electrochemistry instruments were used to make the measurements. Below is a description of the cell and the materials and instruments used to build and operate it.

2.1   Materials

The gases used in this work, nitrogen (99.99%), oxygen (99.9+%) natural gas (94% methane) and hydrogen (99.995%) came in compressed gas cylinders supplied by BOC. The gas flow rates were controlled individually with mass flow controllers supplied by Platon. All the metal salts used in this work were metal chlorides and were obtained from the Aldrich chemical company and used as supplied. The metal electrodes were obtained from Advent research materials ltd. UK and were also used as supplied. The used electrodes were recycled. The aqueous solutions were prepared with deionised water from a Milli-Q plus (>0.05 S cm^{-2})water purifier.

2.2   Instruments

The electrical measurements taken in this work were made with standard electrochemistry instruments. A buffer amplifier (input impedance of 100 MΩ provided by Mr R. Waymark UCL) in conjunction with a digital storage oscilloscope (Tektronix TDS 3021) was used to record the potential difference measurements. These measurements were typically 40 seconds long at a frequency of 100 Hz, this data was then averaged with the standard deviation taken as the error. A computer-controlled potentiostat (µAutolab, Eco-Chemi, Windsor Scientific, UK), was used to record the current-potential scans, running with GPES software. The data was then transferred a PC and manipulated using Microsoft

Excel or Sigmaplot 5.0. The electrode surface temperatures were measured using an optical pyrometer with a resolution of $\pm$ 20 ^{0}C (I.P.Parkin, UCL) or a thermal imaging pyrometer (Mikron, M9100) with a typical error of $\pm$ 1.3 – 2.8 ^{0}C, see figure 2.7.

2.3 The Burner

The burner used in these experiments was specially designed and was built in house here at UCL. Its design was based on that of a Meker burner. A Meker burner has several orifices in the burner top plate for the gases to exit see figures 2.1 and 2.2
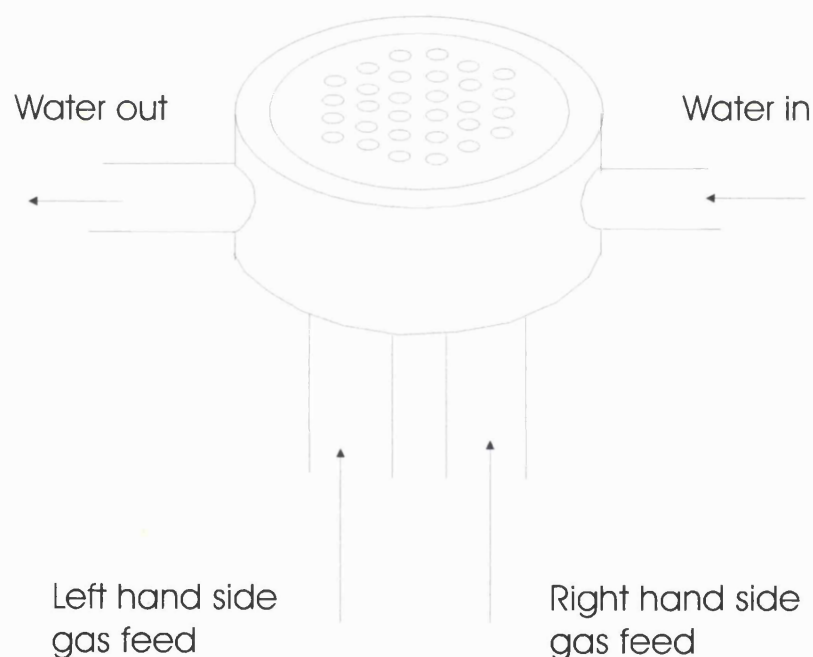
Figure 2.1 Shows the Meker type burner designed for these experiments, with its water-cooling system and dual gas flow capability. Also shown is the hexagonal array of the gas exit orifices.

The burner used in this work had 30 such orifices. Above each of these orifices an individual PRZ cone is created from the reacting gases. As the gases travel downstream the PRZ cones merge and form a secondary reaction zone (SRZ). This SRZ part of a Meker flame is isothermal, and is homogeneous through its cross-section and was chosen for this work for these reasons.

The burner was mounted on an earthed aluminium table and was water-cooled because of the high temperatures and prolonged usage it was exposed to. The burner design included the capability to deliver two different streams of gas at equal rates, to the burner head simultaneously, as can be seen in figure 2.1. The two gas streams were then combusted to produce one controlled flame at the burner top plate.

2.3.1   The Burner top plate

The orifices in the brass burner top plate were hexagonally arranged in the formation 4:5:6:6:5:4, with each half having 15 orifices of 0.5 mm diameter separated by 0.5 mm, figure 2.2 A. This design was based on a template supplied by Prof. A. N. Hayhurst, University of Cambridge. The two centre rows (6:6) were separated by a 1.0 mm gap in order to bridge the septum between the two internal chambers in the burner. The two halves of the burner needed to be identical; this ensured that the two gas streams entering the burner could also escape at equal rates, ensuring the gas exit velocity on each side was equal. Figure 2.2 shows a plan view of the burner top plate and the arrangement of the orifices (A). Also shown is a plan view of the burner with the top plate removed, it shows the two internal chambers of the burner with their two separate gas feeds (B). Also indicated is the water-cooling system, which is necessary for the reasons mentioned above.

Gases in Water cooled
jacket

Septum

A B
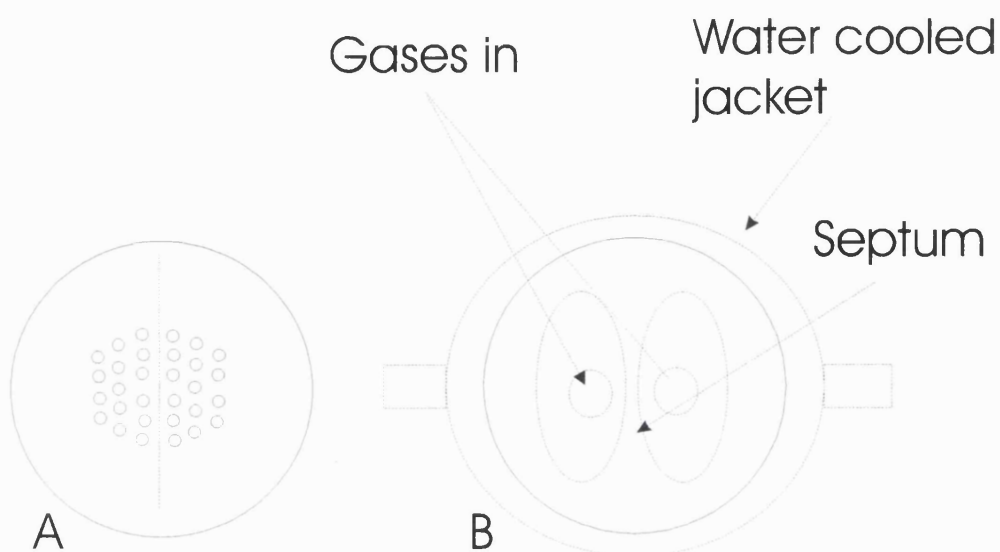
Figure 2.2 Schematic of (A) the burner top plate with a hexagonal arrangement of gas exit orifices and (B) the internal chambers of the burner surrounded by a water-cooled jacket.

2.4 The burner manifold

The burner manifold shown schematically in figure 2.3 was constructed from Low Density Poly Ethylene (LDPE) tubing, with a 4.2 mm internal diameter 6.4 mm external diameter supplied by Goodfellows, (U.K.). All the joints were secured with wade or swagelock fittings. Both sides of the manifold need to be identical in order for the gas flow rates and thus the flame on each side of the burner to be identical. The gas flow rates between the cylinders and the mixing chambers, for each individual gas, was controlled by a separate mass flow controller which allowed the ratio of gases to be altered The nitrogen pipelines were interrupted between the supply and the mixing chambers by round-bottomed flasks (RBF), which allowed metal salts to be added to the flame. A schematic of the manifold is shown in figure 2.3.
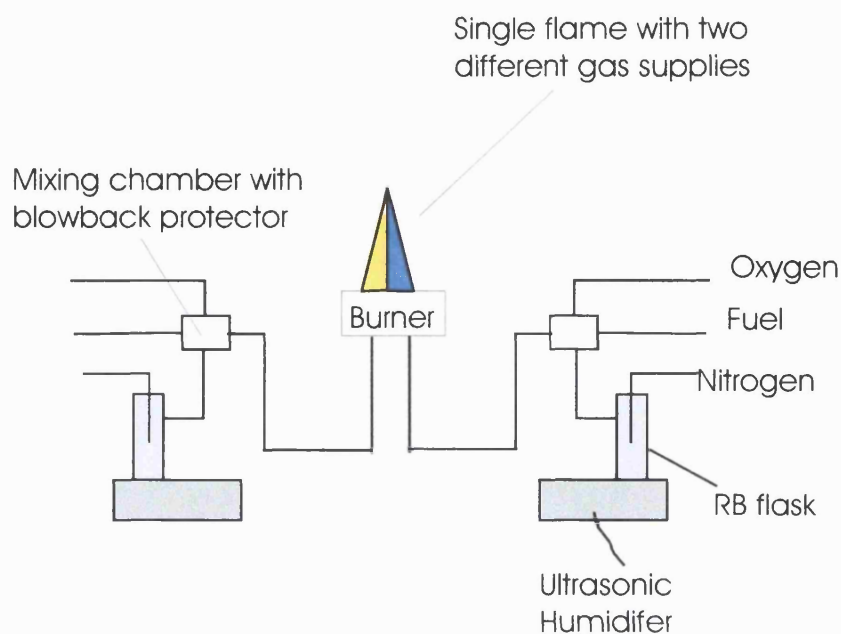
Figure 2.3 A schematic of the burner used in this work, shown are the dual manifolds used to create the two flames at the burner head. Also shown are the ultrasonic humidifiers used to aspirate metal salt solutions into the flame gases.

2.4.1 Addition of metal salts to the flame

Solutions of metal salts can be added to the specially designed RBFs, shown in figure 2.4. From the RBF's it was possible to aspirate solutions of metal salts into the gas stream. Ultrasonic humidifiers were used to aspirate the metal salt solutions; here a vibrating plate (> 20 000 Hz) creates tiny droplets of solution suspended in the air above the solution that the plate is immersed in. The suspended droplets are then carried away in the nitrogen gas stream in a consistent manner, which is achieved approximately 20 seconds after the humidifier is switched on. The solutions in the RBFs could be replaced or diluted through the injection port while the burner was being operated. Measurements of the rate of removal of the solutions in the RBF were made and found to be 8.0 cm^{-3} of solution removed per hour of

operation at a nitrogen gas flow rate of 1.0 L min^{-1}. The range of concentrations of solutions that can be used in this system is limited to between, 0.1 M and 1.0×10^{-7} M. This is because any concentration higher than 0.1 M tends to block the orifices in the burner top plate and concentrations lower than 1.0×10^{-7} M produced responses that are outside the limit of detection of the instruments.
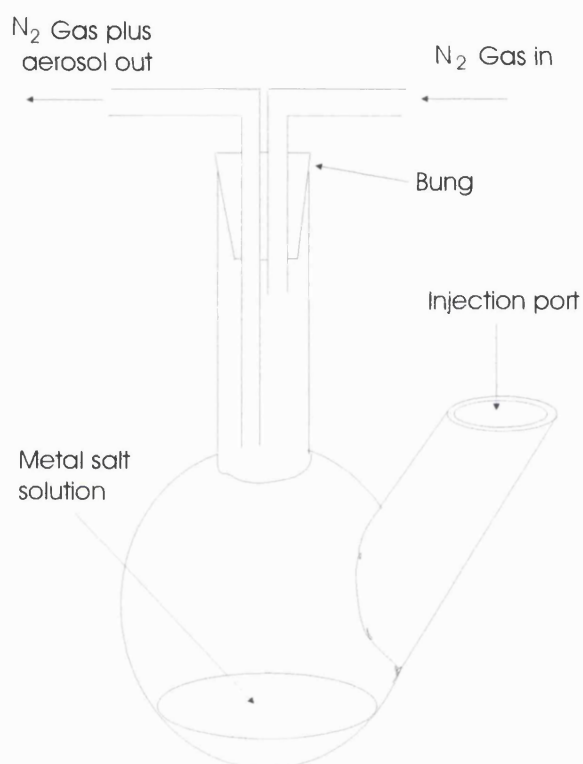
Figure 2.4 A schematic of the specially designed round bottomed flasks used for introducing metal salts solutions to the flame gases.

2.4.2   The gas mixing chambers

The gas mixing chambers used in this work were specially designed and are shown schematically in figure 2.5. The mixing chambers were fitted to the manifold as a safety precaution, because when working with mixed combustible gases the potential for explosions is high. The mixing chambers were capable of taking three

different gas streams, H_2, O_2 and N_2 which contained the aerosol of metal salt solutions, mixing them and then delivering them to the burner feed pipe.
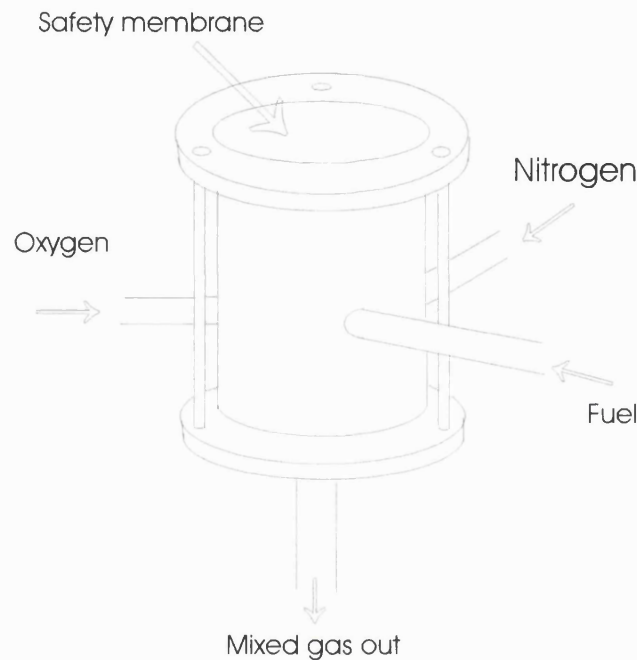
Figure 2.5 Shows the gas-mixing chamber designed for this project, which is capable of mixing three different gases and delivering the mixed gas to the burner.

The mixing chambers were fitted with a safety membrane that failed in the event of a blowback explosion. Blowback explosions happen due to the lowering of the gas flow velocity (pressure inside the manifold) this gives the flame front, which has its own characteristic velocity at different fuel/oxidant ratios[53], a chance to travel inside the manifold and thus cause an explosion. When such an explosion happens the failure of the safety membrane ensures the rapid gas expansion that results is dissipated safely.

The mixing chambers also had a reservoir (2-3 cm^3) for collecting any excess solution that may condense inside the manifold, which prevented pipe blockages due to excess solution.

2.5 A description of the flame created with this burner

The flame created with this burner system was approximately 1 cm in diameter and approximately 10 cm tall at atmospheric pressure. An image of the flame is shown in figure 2.6 and its physical parameters are tabulated in tables 4 a and 4 b.

Secondary Reaction Zone (SRZ)

Primary Reaction Zone (PRZ)
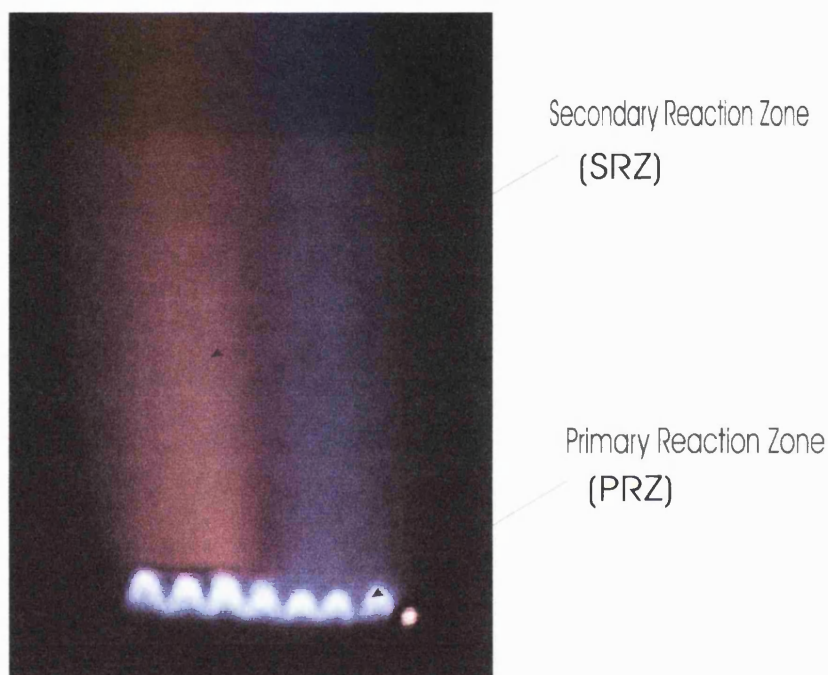
Figure 2.6 This photo shows the two flames that comprise the flame electrochemical cell used in this work. The left hand side (LHS) compartment contains 5 mM NaCl and the right hand side (RHS) shows the natural (CH_4) flame.

A description of the flame now follows. A clear area (pre-heat zone) approximately 0.5 mm separated the burner plate and the PRZ cones. These bright luminous cones extended approximately 4 mm above the burner head and are approximately 0.1 mm thick at atmospheric pressure[54]. The SRZ or burnt gas region of a flame, created with a Meker burner and premixed gases, has laminar flow and is isothermal, and chemically homogenous through its horizontal cross section.

Table 4. A and B shows some of the physical characteristics of the flames used in this work.

A

Property	Value
Equivalence ratio (fuel-rich)	1.334
$H_2/O_2/N_2$	2.67 / 1.0 / 1.67
Total unburnt gas flow	5.34×10^{-5} m^3 s^{-1}
Total gas exit area	5.9×10^{-6} m^2
Velocity in the burnt gas v_r	28.44 m s^{-1}
Adiabatic flame temperature	2920 K
Electrode surface temperature (thermal imaging pyrometer)	1800 K
Flame diameter	8.0 mm
Flame cross-sectional area	5.02×10^{-3} m^2

B

Property	Value
Equivalence ratio (stiochiometric)	1.0
$CH_4/O_2/N_2$	0.8 / 1.6 / 0.8
Total unburnt gas flow rate	3.2×10^{-4} m^3 s^{-1}
Total gas exit area	2.9×10^{-5} m^2
Velocity in the burnt gas	11.0 m s^{-1}
Adiabatic flame temperature	2932.4 K
Electrode surface temperature (hand held pyrometer)	1690 K
Flame diameter	8.0 mm
Flame cross-sectional area	5.02×10^{-3} m^2

Figure 2,6 shows a photograph of the methane flame with NaCl 5 mM added to the left flame, the two distinct compartments of the cell are visible and also the interface between the two flames. Both flames are fed by equal gas flow rates.

2.6   The choice of electrodes in a high temperature electrochemical cell

The working and reference electrodes used in this work were mostly 1.0 mm diameter platinum wire. All of the other high melting point metals that were available were assessed as working and reference electrodes for use in this gas phase cell but for various reasons all except platinum proved unusable. For instance the first row transition metals Sc, Ti, V, and Cr all formed oxides on their surfaces when inserted into the flame, which affected the reproducibility of the measurements made with electrodes made of these materials. The rest of the first row transition metals Mn, Fe, Co, Ni, Cu, and Zn all melted instantly on insertion into the flame.

The second row transition metals Nb, Mo and Ru lasted a little longer in the flame but the flame had an eroding (etching) effect on the electrodes which made them grow smaller and eventually retreat from the flame altogether. The measurements taken with these electrodes were stable but superimposed on decline in magnitude due to the electrode becoming smaller. The third row transition metals Hf, Ta and W had similar responses to the second row transition metals in that they oxidised and dissolved into the gas phase. Molybdenum and tungsten were chosen as the two best sacrificial electrodes as they dissolved at a steady rate and produced a stable potential.

Tungsten interestingly, which is the electrode material of choice in high temperature gas phase electrochemical measurements, was found to split when inserted into the flame, this subsequent increase in electrode surface area had a predictable effect on the measurements made with this electrode.

The third row transition metal platinum proved to be the most suitable as a high temperature gas phase electrode, provided the temperature in the gas phase environment was not to hot so as to melt the platinum. With platinum probes there was no visible fouling on the electrode surface and any evaporation of the probe over the period of an experiment (ca. 2 hours) was undetectable measuring the difference in mass of the electrode before and after the experiment.
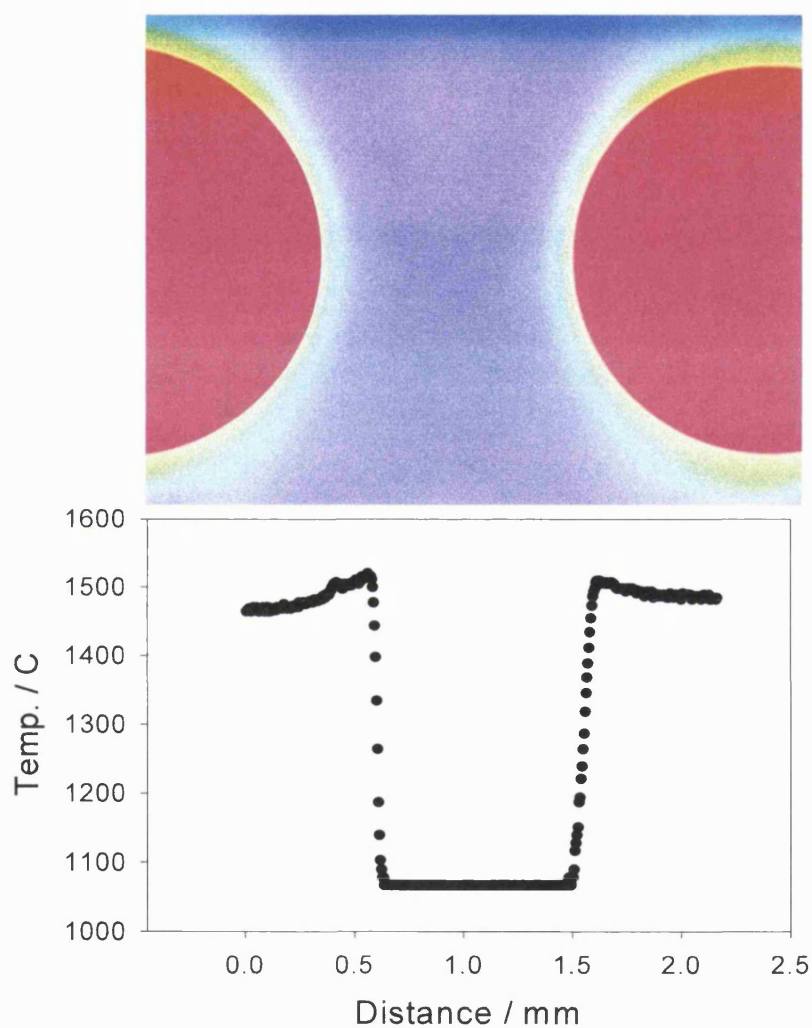
Figure 2.7 A thermal image of two 1.0 mm diameter platinum wire electrodes, with spherical ends caused by melting, immersed in the flame plasma. Also shown is the thermal data associated with the image.

The platinum electrodes did however pick up some gas phase metal species from the flame, which will be discussed further in chapter 3. Figure 2.7 shows a thermal image of two platinum wire electrodes immersed in the flame, also shown is the thermal data associated with the electrodes surfaces.

The counter electrode can be the burner or another probe (a platinum flag) inserted into the flame. The main requirements for the counter electrode are that it has good contact with the flame plasma, and that the area of contact be much larger than that of the working probe. This limits the current passing through the circuit by the current to the smaller working probe.

Each different metal that was assessed as an electrode material was found to established its own unique electrode potential versus a platinum reference electrode placed in the same cell. These electrode potentials are dependant on the metals free energy of atomisation and ionisation.[55],[56], and are caused by the gas phase metals ions at the metal electrodes surface.

2.7   Electrode assembly and positioning

All of the electrodes used in this work were 1.0 mm diameter platinum wire unless otherwise stated. The electrodes were positioned using two x, y and z micropositioners (Physik Instrumente), which had 1μm resolution on each axis. The horizontal axis was motorised and controlled from a PC, which allowed reproducible positioning. The electrodes were positioned 5.0 mm above the burner top plate, with their ends separated by 5.1 mm; this is just at the top of the PRZs in the flame and is also the point of maximum ionisation in the flame. When the platinum electrodes were inserted 2.0 mm into the flame no melting (distortion of shape) took place, when however the electrodes were inserted into the flame to a distance of 4.0 mm the tip of the electrode melted and formed a sphere at the end of the electrode. This transformation had the effect of altering the probes surface area

while retreating from the flame, to an approximate distance of 2.5 mm of electrode still in the flame.

For the diffusion potential measurements two platinum indicator electrodes were inserted into the cell one in each compartment.

For the redox potential measurements two platinum indicator electrodes were inserted into the cell one in each compartment. These two electrodes were used concurrently as a reference electrode and a working electrode in the ion current measurements. A platinum flag 1 cm^2 placed downstream and equidistant from the other two electrodes, served as the counter electrode in the ion current measurements. A schematic diagram of the electrode can be seen in figure 5.1, chapter 5.

2.8   Operation of the cell

Solutions of metal salts were introduced into the flame in the following way. A mist was generated from the metal salt solution in the RBF by the ultrasonic humidifier, nitrogen gas was then passed through the mist and subsequently some of the mist droplets are carried along with the nitrogen gas to the mixing chamber, see figures 1.12, 1.13 and 1.14. Here the nitrogen gas carrying the droplets of salt solution combines with the fuel and oxygen. The mixed gases are then brought to the reaction zone at the burner head where they are combusted. *Care should be taken when working with mixed combustible gases and measures should be taken to avoid explosion.* It was found from a calibration experiment that 8 ml of solution were being removed from the round bottom flask per hour. But it is unclear how much of this solution is actually carried into the flame due to condensation of the liquid on the walls of the flow system.

3.0 Electrochemical measurements in a gaseous electrolyte.

The ultimate aim of this project was to develop the controlled electroduction of gaseous ions. This was to be achieved by analysing the VAC's obtained in an unseeded flame using a three electrode set-up. And then re-examining the VAC obtained in the same flame after a metal salt had being introduced into the flame. Here it was hoped that reduction waves associated with the cations present in the flame could be resolved.

The material presented in this chapter includes our attempts at dynamic electrochemistry and includes details of conductivity measurements. The characteristics of flame temperature are described and the relationship between temperature, ionisation level, stiochiometry and potential is presented and discussed. The effect of inserting the electrode into the flame is also discussed and the results of an investigation of absorption/adsorption of flame borne species on/into the electrode are presented.

3.1 Attempts at Dynamic Electrochemistry

Using analysis of the VACs as a starting point attempts were made to electroreduce gas phase metal ions at the surface of a platinum electrode that was inserted into the flame. Platinum was used as the working electrode here because it is stable (does not evaporate/ dissolve/oxidise) when inserted into the flame. A platinum flag, (1 cm^2) was used as a counter electrode, this was placed approximately 5 mm above the WE and RE, which were, placed 5.0 mm above the burner top plate. Various metals were used as reference electrodes; the complete list and their responses are detailed in the experimental section 2.6. Molybdenum wire (2.0 mm diameter) was used as the reference electrode in the following experiment because it produces the most stable potential when inserted into the flame and it is relatively cheap. Flame B was used for this experiment (see introduction).

Figure 3.1 shows the VAC's obtained using the three-electrode set-up described above. The blue line is the VAC recorded in the unseeded flame and the black line is the VAC was recorded in the same flame, which was seeded with 0.25 M $CuCl_2$. The molybdenum reference electrode was placed in the left side of the flame, which was kept constant (i.e. no additives and gas flow rates kept constant). The copper solution was aspirated into the right side of the flame where the working electrode was placed. The scan rate here was 1.0 V s^{-1} in a cyclic voltammetry experiment and the plot, figure 3.1 includes both the forward and backward scans, which line up perfectly.
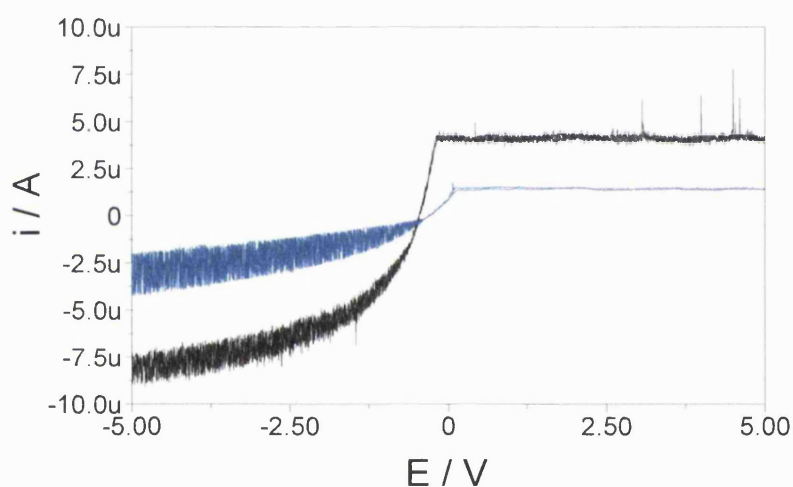
Figure 3.1 Shows the current voltage scan in a natural unseeded $CH_4/O_2/N_2$ flame, (blue line) and the current voltage scan in the same flame seeded with 0.25 M $CuCl_2$ solution (black line). A 1.0 mm diameter platinum wire was used as a working electrode; a 2.0 mm diameter molybdenum wire was used as the reference electrode. These electrodes were placed 5 mm above the burner and 5 mm apart. A platinum flag 1 cm^2 was used as a counter electrode and was placed 5 mm above the reference and working electrodes.

It is known from the work of Butler and Hayhurst[57] that the ions created when copper is introduced into a flame include Cu^+ and a range of copper hydrate ions and copper oxide ions (see introduction). The presence of these copper-containing ions is also visible in the VAC's in figure 3.1, where the increase in the (transport limited) cation current is due to the increase in total ion concentration in the flame.

The flattening of the current voltage characteristic on the positive potential side in figure 3.1 is due the electron current saturating the electronics in the potentiostat.

This experiment was repeated using the $H_2/O_2/N_2$ flame and platinum wire (1.0 mm diameter) as the reference electrode. The result can be seen in figure 3.2, again we see the VAC associated with the unseeded flame and the VAC associated with the flame seeded with 1.0 mM CsCl.
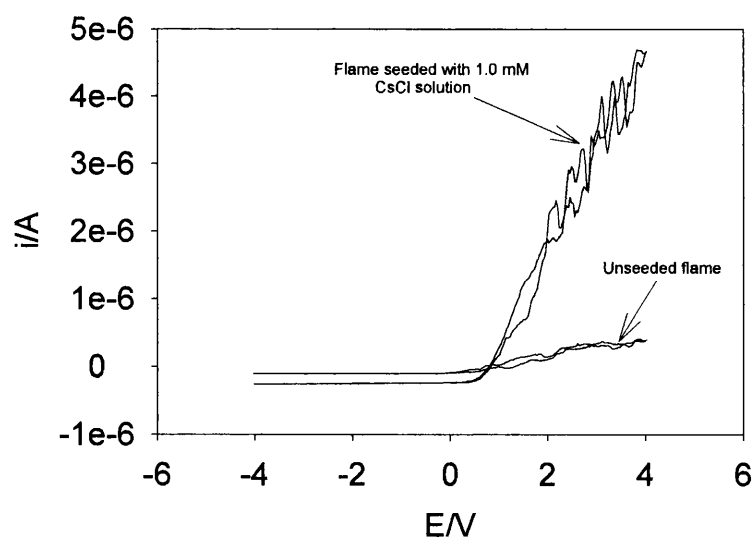
Figure 3.2 The increase in ion and electron currents on the introduction of a 1.0 mM solution of CsCl into flame A, obtained using the electrode set up described in the text.

In figure 3.2 the limiting cation current can be seen for both the seeded and unseeded flames, but no reduction wave associated with the added species is

identifiable. The current is due to the total ion concentration. In figure 3.2 the increase in electron current is also visible. These extra electrons are a product of the ionisation of the added species, equation (44),

(44) $M \rightarrow M^+ + e^-$
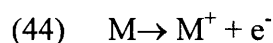
Again the current here is due to the total concentration of electrons, as one would expect.

The main point here is that, in the voltammagrams recorded using this experimental set-up, between $-5V$ and $+5$ V and shown in the examples above, is that there are no features that resemble or can be described as reduction waves or oxidation waves which corresponds to the reduction or oxidation of ions present in the flame. In the above examples figures 3.1 and 3.2, the transport limiting cation current i_l in the unseeded flames is due totally to natural flame ions like H_3O^+ (blue line in figure 3.1). In the seeded flames however the limiting cation current, $i_{l(s)}$ is due to the natural flame ions (H_3O^+) and to the ions created due to the introduced species[58],[59] (e.g. Cu^+). There will be a higher background current in figure 3.1 because a CH_4 flame was used compared to figure 3.2, which was a H_2 flame.

3.2   The relationship between temperature, stiochiometry and conductivity

The temperature of the PRZ of our flame B was calculated using a programme developed at Cambridge University[60],[61],[62], based on the enthalpy change, ΔH, between the reactants and products. The temperature of a platinum electrode inserted into the same flame 5 mm above the burner top plate was also measured using a thermal imaging camera. Comparison of the calculated adiabatic flame temperature and the measured platinum electrode surface temperature in figure 3.3 reveals huge losses in temperature between the PRZ of this flame and the electrode surface. This loss of temperature can be accounted for by heat radiation and

conduction by the platinum electrode. Here the temperature is plotted against the ratio of oxygen to hydrogen used to feed the flame.
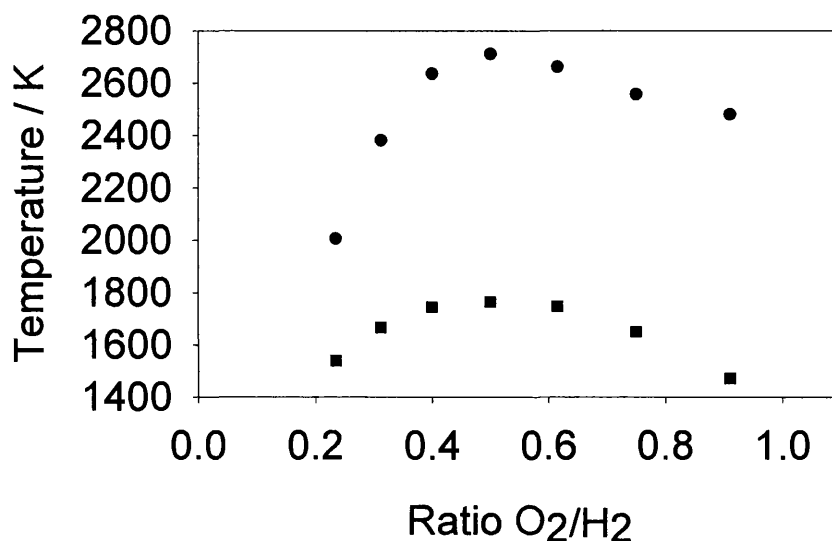
Figure 3.3 Plot of calculated flame temperature (•) in the PRZ of our flame B versus the oxygen/hydrogen ratio. Also shown is the temperature measured at the electrode surface (■) versus the oxygen/hydrogen ratio.

In the figure 3.3 the maximum temperature, both measured and calculated, is achieved at a stiochiometric ratio (i.e. 1 oxygen molecule to 2 hydrogen molecules). The plot shows that the difference between the two temperatures is of the order of 1000 K, which is quite a considerable margin. If the measurement was taken with the electrode inserted into the PRZ of the flame the measured temperature would be higher, however in practice the platinum electrode melts when inserted into the PRZ of this flame system.

Another interesting plot is figure 3.4. This is the plot of ion current at − 4 V versus the oxygen/hydrogen ratio. As the ion current is directly proportional to the concentration of ions in the flame, this plot gives us the ratio, O_2/H_2, of the gas mixture in which the maximum number of ions will be available. The current here

should be taken as a relative measure of ion concentration, as the absolute value depends on the electrode surface area, which was an experimental variable for each experiment.
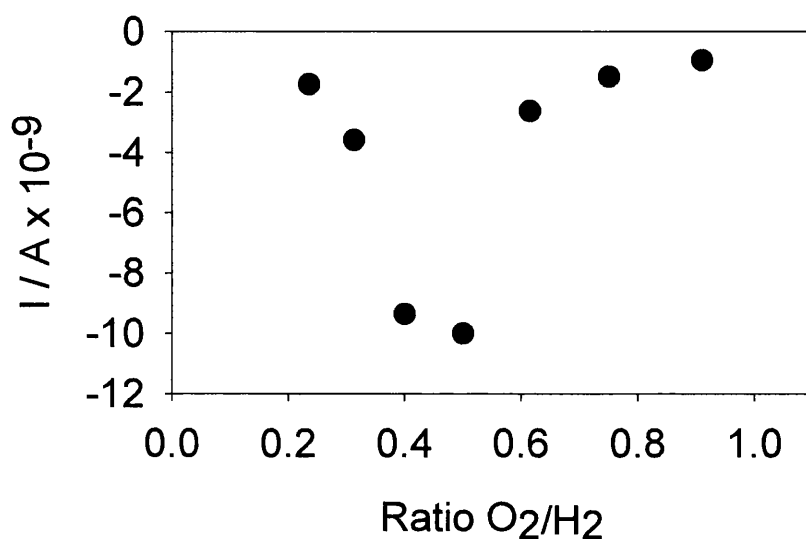
Figure 3.4 Plot of ion current at – 4 V versus the oxygen/hydrogen ratio used in the feed gases. The ion current measurement was made using a three electrode system, a 1mm platinum wire WE and a 1 mm platinum wire RE and a 1 cm^2 platinum flag counter electrode. The WE and RE were placed 5 mm above the burner and the CE 5 mm above the WE and RE.

Another experiment was performed using the dual burner in which the ratio of oxygen/hydrogen was left constant in the left side of the flame (see experimental section) while the ratio of oxygen/hydrogen was varied in the right side of the flame. Here two platinum indicator electrodes were inserted into the flame one in each side and the potential difference between them measured. Figure 3.5 shows the plot of potential difference measured between the two electrodes versus the ratio oxygen/hydrogen fed into the right side of the flame. Care was taken in this procedure to make sure that the total gas exit velocity did not change from

measurement to measurement; differences in the flame front velocity (burning velocity) due to the different O_2/H_2 ratios were neglected.

WARNING Altering the fuel/oxidant ratio in any burner system is extremely dangerous, and normally results in explosion or the flame being blown out.
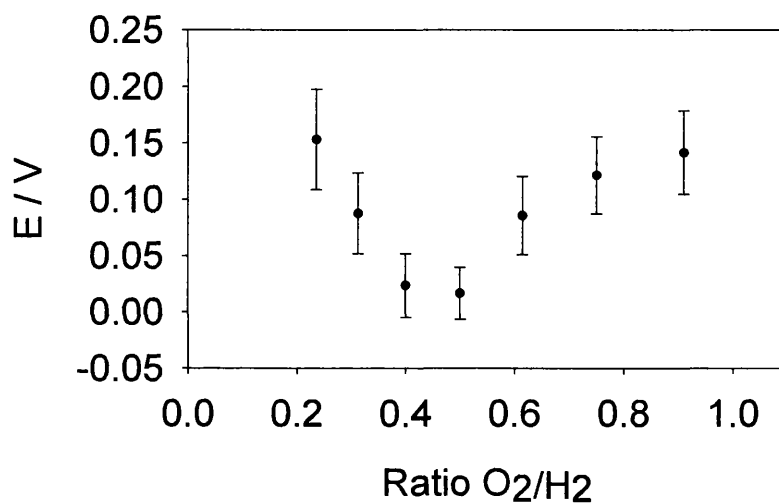
Figure 3.5 Plot of potential difference measured between two indicator electrodes inserted into the flame one in either side versus the ratio oxygen/hydrogen gases fed into the right side of the flame.

Figure 3.5 shows that as the ratio oxygen/hydrogen becomes more stiochiometric and thus the concentration of ions in both sides of the flame become equal the potential difference disappears. This potential difference is likely to be a diffusion potential following the extent of ionisation, and is discussed further in chapter 4.

Figure 3.6 shows the VAC's measured using the three electrode set-up described above (section 3.1). The difference between the VAC's in figure 3.6 is that the platinum working electrode is inserted different distances into the flame for each VAC. The act of moving the electrode further into the flame has two effects. Firstly

the separation between the WE and the RE becomes shorter thus reducing the resistance between the two electrodes. Secondly, the further the WE is inserted into the flame the more surface area of electrode is in contact with the flame.
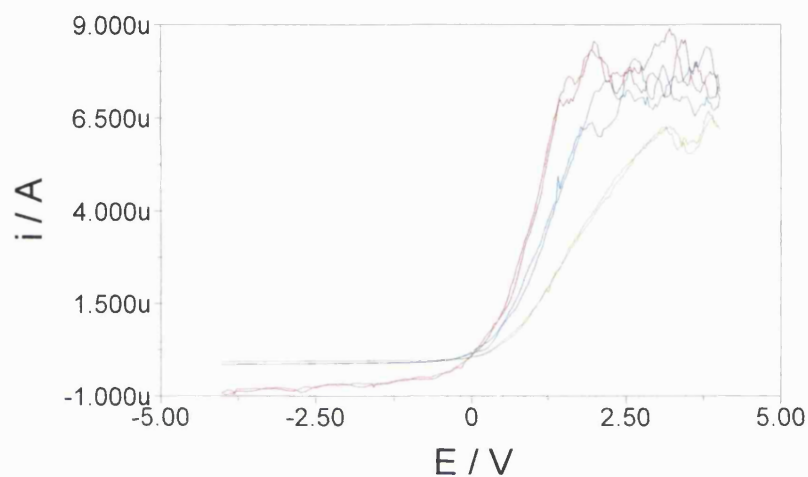
Figure 3.6 Plot of the VAC's generated using a three electrode system described in the text with the WE inserted different distances into the flame. Green 1 mm, blue 2 mm and red 3 mm.

The shift in the coulombic exchange region in the VAC's in figure 3.6 is due to the change in resistance between the two electrodes due to them becoming closer. The separation between the RE and WE are 6 mm for the green line, 5 mm for the blue line and 4 mm for the red line. In figure 3.6 we can also see the currents becoming larger due to the increased surface area of the electrode. The area of the electrode exposed to the flame increases as the electrode is inserted further into the flame, for the green line in figure 3 the electrode was inserted 1 mm in to the flame, for the blue line 2 mm and for the red line 3mm.

3.3   Ion current versus concentration of salt solution added to the flame

The ion current measurements in figure 3.7 were made using a three-electrode system with varying concentrations of KCl added to the flame. The electrodes consisted of two platinum wire electrodes, 1 mm in diameter that were inserted into the flame cell, one in each side 5 mm above the burner and 5 mm apart. The platinum wires formed a small sphere at their tip on insertion into the flame, approximately 1.5 mm in diameter. A platinum flag (1 cm^2) was placed downstream equidistant from both the working and reference electrodes and was used as a counter electrode.
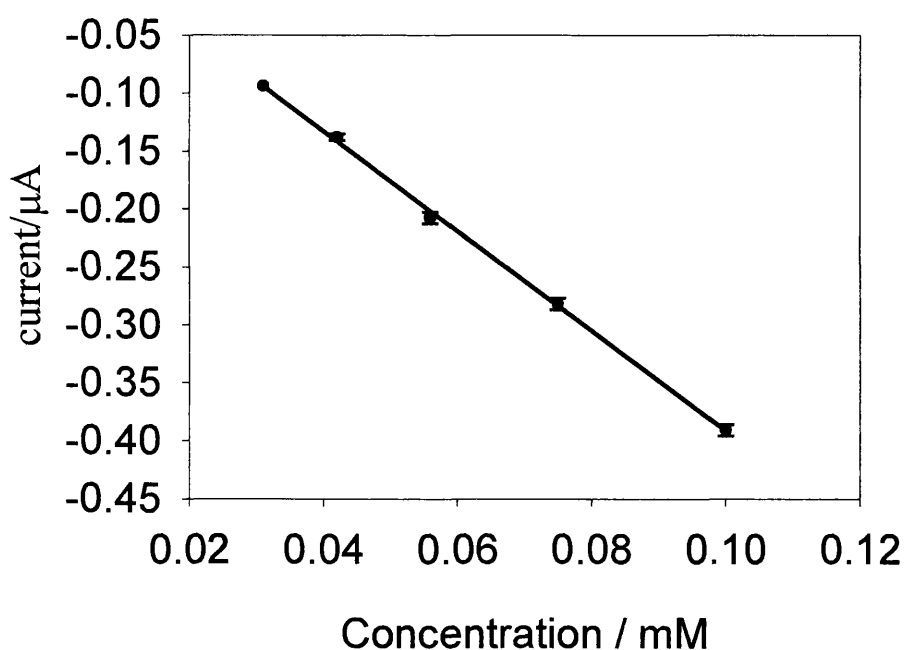
Figure 3.7 A plot of ion current at – 5 V versus concentration of KCl solutions introduced into a $H_2/O_2/N_2$ (01.6:0.6:1.0, L min^{-1}) flame. The line is the best fit least squares straight through the data. The error bars are the standard deviation.

The ion current was measured at – 5 V. Each measurement was taken three times and averaged. The error bars in figure 3.7 are based on the standard deviation of three measurements. The scan rate was 1.0 V s^{-1} between – 5 V and + 5 V. A linear

relationship is apparent over the concentration range shown. At higher concentrations of salt solution the dependence on the ion current approaches a saturation point. The actual concentration of ions can be estimated from the ion currents and the equations presented in chapter 1, but are considered here as relative measurements, which are proportional to the ion concentration in the flame.

3.3.1 Conductivity across the gas/gas interface

Using the dual burner described in the experimental section, the conductivity of the flame was measured across the gas/gas interface between the two flowing flames. Figure 3.8 shows a plot of conductivity versus distance through the interface from low concentration in an unseeded flame (LHS) to high concentration in a flame seeded with 0.1 mM CsCl (RHS).
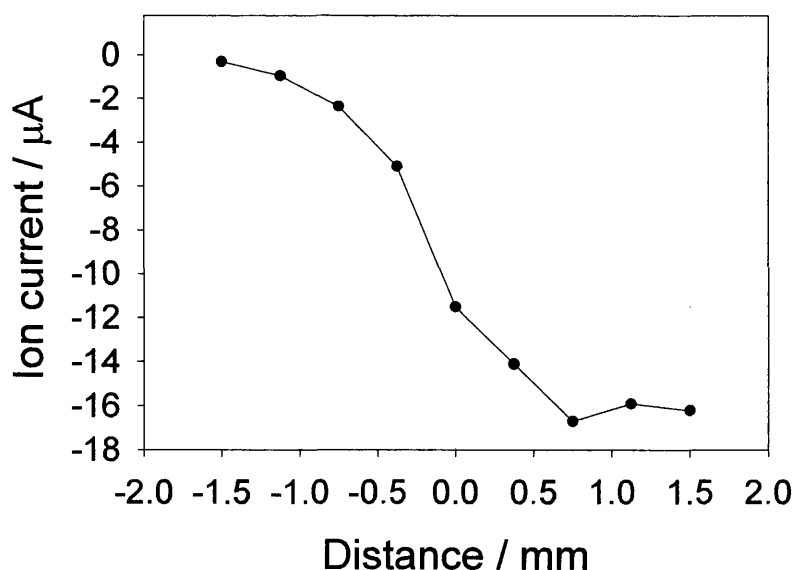
Figure 3.8 Plot of conductivity versus position across the gas/gas interface. The conductivity measurements were made using a two-electrode system, shown schematically in figure 1.6. The WE was a 1 mm diameter platinum wire, and the burner acted as a joint CE/RE.

This experiment used the Langmuir probe set-up shown schematically in figure 1.6. This involved using a 1 mm diameter platinum wire WE, placed 5 mm above the burner surface and using the burner as a joint CE/RE. The working electrode was moved through the interface at 0.3 mm steps and the current was measured at each interval. The spatial resolution of this experiment was limited. However the plot (figure 3.8) shows that the electrodes may be placed at least 2 mm from the interface without disturbing the interface.

3.3.2 The salt concentration versus the floating potential (V_f)

The potential that the conductor attains when dipped into an electrolyte, ($\Delta\Phi_{m/s}$ in solutions)[63] is called the floating potential, V_f in plasma physics[64]. This is also true for conductors inserted into a flame. Figure 3.9 shows the ion currents measured at different potentials for various concentrations of KCl added to a ($CH_4/O_2/N_2$ (0.8:1.6:0.8, L min^{-1}) flame. These measurements were made using a three electrode system, at a scan rate of 1.0 V s^{-1} between + 3 V and − 3 V. The platinum wire working electrode was placed in the left cell where the metal salts were to be aspirated. The platinum reference electrode was placed in the right side of the flame. Both of these electrodes were positioned 20 mm above the burner and 5 mm apart. A platinum flag 1 cm^2 was used as a counter electrode and was positioned approximately 5 mm above the other two electrodes (downstream).

The floating potential (V_f), the point where no current (ion or electron) is flowing can be seen to shift to a more negative value with the increase in (KCl) ion concentration. The shift is from − 0.41 V in the natural unseeded flame to − 0.75 V in the flame seeded with 0.1 M KCl solution. The shifts are due to the increase in the concentration of ions and electrons in the flame. The reason the potential becomes more negative is because of the higher mobility of electrons relative to ions, i.e. more electrons reach the probe than cations. This phenomenon was investigated with the aid of the dual burner mentioned in the experimental section
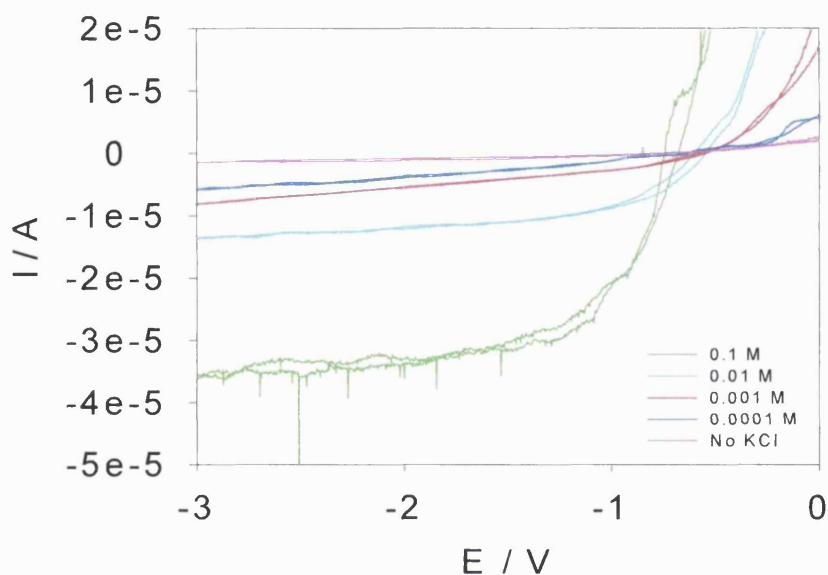
Figure 3.9 Comparison of the different ion current response on the introduction of different concentrations of KCl into a $CH_4/O_2/N_2$ (0.8:1.6:0.8, L min^{-1}) flame, obtained using a 1.0 mm platinum wire electrode placed 20 mm above the burner versus a platinum wire reference also 20 mm above the burner and a platinum flag (1 cm^2) counter electrode 25 mm above the burner. The electrode surface temperature was measured at 1690 K.

(2.3) and was found to be related to a diffusion potential and is discussed further in chapter 4. It was also found that changing the metal salt species also resulted in a shift of the floating potential of the flame. This was found to be related to the redox potentials of the gaseous ions and is discussed further in chapter 5.

3.4 Adsorption and absorption of flame borne species by platinum electrodes.

With the high temperatures encountered in this work it is reasonable to assume that there is penetration of flame borne species into the bulk of the platinum electrodes. These absorbed species will include both natural flame species and the introduced (metal) species. Electron probe microscopy was carried out on the electrodes that were inserted in the flame for electrochemical measurements to see to what extent absorption had occurred. The results and experiments are presented below.

A 1 mm platinum wire electrode was inserted into flame A, 5 mm above the burner. The flame contained the vapour of a 0.1 M solution of $CuCl_2$ and the electrode was left in place for one hour. The electrode was then mounted using a quick drying epoxy resin. The end of the electrode that was inserted into the flame was polished to reveal a cross section. The electrode was polished with 1.0, 0.5 and 0.25-micron polishing paper until a smooth ridge free surface was attained.

Using electron probe microscopy, an elemental analysis was performed on the cross section to see to what extent the copper had absorbed into the platinum. The results showed that copper had been absorbed equally throughout the electrode at a level of 0.35%, see figure 3.10, with possible peaks in the distribution of copper towards the central core and towards the surface of the electrode.

At this temperature the platinum is glowing red-hot and temporarily melts to form a sphere at its tip. This melting process may give the platinum electrode a chance to absorb some of the gas phase copper species. The even distribution suggests some kind of equilibrium amount of alloying between copper and platinum at this temperature. We do not expect to see much copper on the surface of the electrode as the m.p.'s of copper (1356 K), CuO (1599 K) and Cu_2O (1508 K) are lower than the electrode surface temperature, (1690 K) and therefore any copper species that

deposits onto the surface while the electrode is immersed in the flame would evaporate instantly.
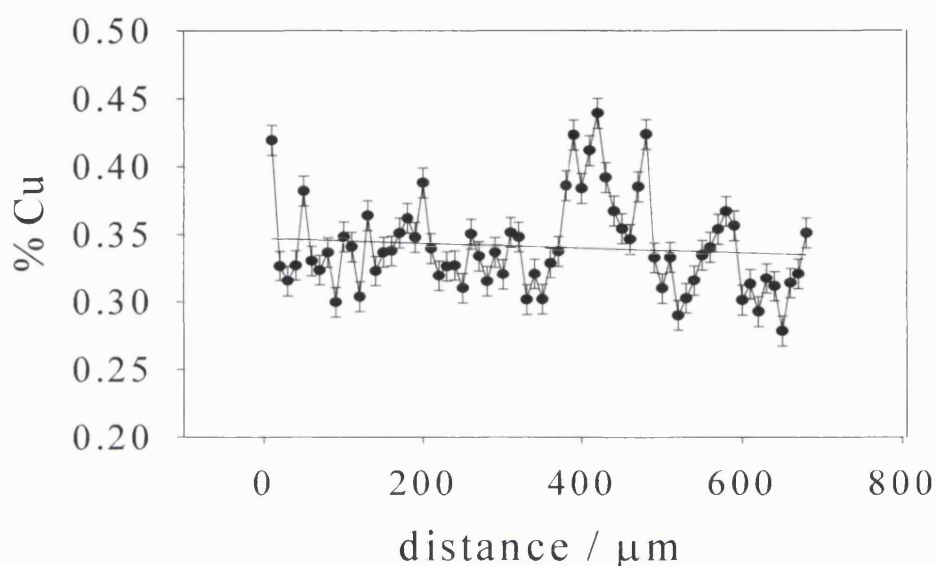
Figure 3.10 The distribution of copper through part of the cross section of a 1 mm diameter platinum wire electrode, which was exposed to a ($CH_2/O_2/N_2$ (0.8:1.6:0.8, L min^{-1}) flame, which was seeded with a 0.1 M $CuCl_2$ solution for one hour.

3.4.1   The effect of applying a potential to the electrode

To find out what effect applying a potential to an electrode inserted into a flame has on the extent of absorption of gas phase metal species, an experiment was designed in which four electrodes were inserted into a ($CH_4/O_2/N_2$ (0.8:1.6:0.8, L min^{-1}) flame. Each of these electrodes was held at a different fixed potential relative to another platinum wire electrode also in the flame, and are listed below,

1, platinum electrode (open circuit) with no copper in the flame.

2, platinum electrode held at –4V with copper in the flame.

3, platinum electrode held at +4V with copper in the flame.

4, platinum electrode (open circuit) with copper in the flame.

The electrodes were positioned 25 mm above burner and the potential applied relative to another platinum wire reference electrode also positioned 25 mm above the burner 5 mm apart from the working electrode. The flame was seeded with a 0.1 M solution of $CuCl_2$ and the electrodes left in place for 10 minutes. The working electrodes were flattened on their top side to keep track of their position in the flame, and to make it possible to examine the same part of each electrode. They were positioned 25 mm above the burner top plate in a cooler part of the flame to prevent excessive melting. The electrodes were removed from the flame while the potential was still being applied; this was to avoid any deposits being stripped from the electrode surface due to a change in potential.

The results obtained in this experiment are displayed in figure 3.11. The three electrodes that were exposed to the flame seeded with copper, absorbed copper. The electrode that was biased at – 4 V absorbed the most copper, the electrode on open circuit absorbed a little less and finally the electrode that was biased at + 4 V absorbed the least amount of copper. Also shown for comparison is the electrode exposed to the unseeded flame.
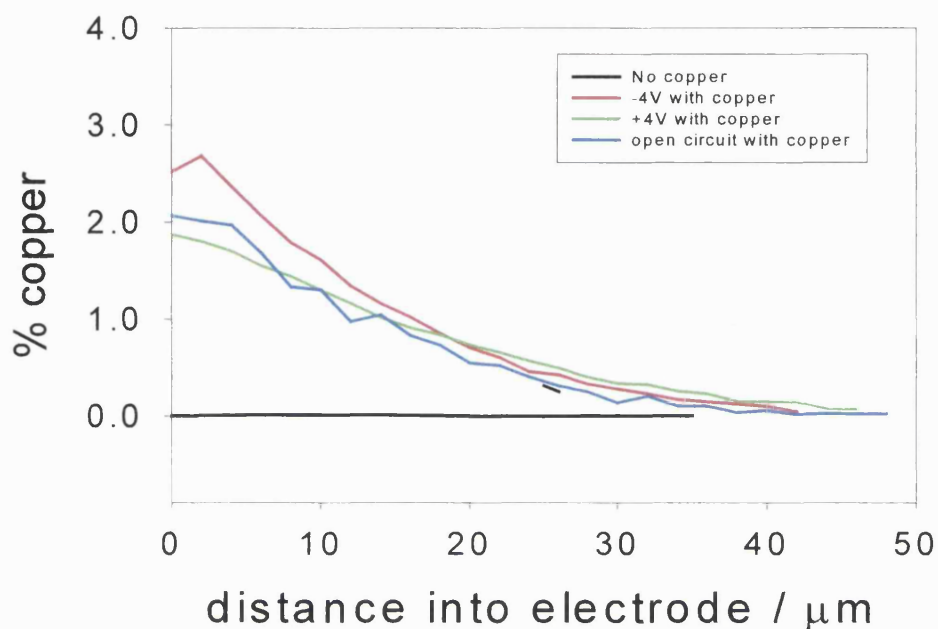
Figure 3.11 The distribution of copper through the first 40 μm of four 1 mm diameter platinum electrodes, inserted into a copper seeded ($CH_4/O_2/N_2$ (0.8:1.6:0.8, L min^{-1}) flame 25 mm above the burner. The electrode surface temperature was measured at 1690 K. Each of the four electrodes was biased differently, (red in the plot) – 4 V, (blue) open circuit and (green) + 4 V. The black line in the figure had no copper in the flame. The measurements were made in that part of the electrode that was directly impinged on by the flame. The relative error in these measurements is less than the line thickness ($\pm 0.02\%$).

Elemental Images were made of two of the electrodes, the one, which contained no copper, and the one, which was biased at –4V, which did contain copper. The images are shown in figure 3.12, a and b respectively. The absorbed copper (pink and white) is visible throughout the platinum (yellow) electrode in image b and appears to be concentrated close to the surface (white). And for comparison a

similar platinum electrode with no absorbed copper, a, which is normally yellow indicating pure platinum.

(a)   (b)

Figure 3.12 Picture (a) shows an elemental image made using an electron beam probe of a pure platinum wire electrode and picture (b) shows the distribution of copper (pink and white) in a platinum (yellow) electrode inserted into a flame seeded with 0.1 M $CuCl_2$ solution and biased at -4 V relative to another platinum electrode in the flame. The electrode surface temperature was measured at 1690 K. A more concentrated distribution of copper is visible towards the surface in image (b).

This result shows that the application of a negative potential to an electrode inserted into a flame, relative to another electrode inserted into the flame increases the amount of gas phase species absorbed by the electrode electrostatically. This result indicates that the deposited copper is being deposited in the form of copper ions.

Although the flame will contain both neutral copper species and ionic copper species and both may be deposited onto the electrode just by coming into contact with it, the increase in deposition due to the negative bias on the electrode can only be due to ionic or polarised species being attracted to the electrode surface electrostatically.

3.4.2 The amount of material deposited/adsorbed by the electrode

Deposition of flame borne species onto the surface of an electrode that has been inserted into a flame presents some problems that are difficult to overcome. The major difficulty arises due to the high temperature at the electrode surface, 1690-1800 K in this work. Here any compound that has a lower melting point than the surface temperature cannot physically be deposited, as it will evaporate instantly on contact with the surface of the electrode. This problem can be over come by depositing compounds that have a higher melting temperature than the electrode surface temperature.

Another problem that was encountered was the fact that the amount of material being deposited, using the aspirated metal salt thermal spray deposition method (AMTSD), as used in this work, is very small, so as to make it difficult to detect.

For example, when a 0.1 mM solution of NaCl is being aspirated into the flame gases, 8.0 cm^{-3} of solution is removed from the round-bottomed flask per hour, by the 1.0 L min^{-1} stream of nitrogen gas. So after an hour of operation, approximately 8.0×10^{-7} mol of NaCl has been transferred into the gas phase (flame). The flame cross-section area is ca. 0.78 cm^2 and the electrode cross-section area in the flame including the Debye length that develops as a function of the concentration of cations in the flame and the potential applied to the electrode, is ca. 0.043 cm^2 (length x width). This simple calculation shows that approximately 5.5 % of the total flame borne sodium may come into contact with the electrode, or 4.4×10^{-8} mol of sodium metal may come into contact with the electrode surface over the

duration of one hour. If we now assume that all of this sodium sticks to the platinum electrode's surface, i.e. it has a sticking probability of 1, this results in a coverage of 3.39×10^{16} atoms cm^{-2}, and as a typical metal surface consists of about 10^{15} atoms cm^2, we can end up with a coating approximately 33 atoms thick.

Even in this ideal situation the amount of coverage is minute and when we take into consideration the high temperature and the high kinetic environment of the surface of the electrode we can see that the coverage will be somewhat less than the calculation predicts. With some adaptations this technology could be used to apply coatings to suitable high melting point substrates where the thickness and morphology of the coat can be controlled. Electrostatic Spray Assisted Vapour Deposition (ESAVD) and Chemical Vapour Deposition (CVD) are already a well developed process and will not be investigated further here[65],[66],[67].

3.5   Conclusions

The application of dynamic electrochemistry methodology to ions in the gas phase was found not possible using this flame system. Approximately 2500 attempts were made to resolve reduction or oxidation waves using various metals as reference electrode (sacrificial Mo and inert Pt) and examining for several different gas phase ionic species. But in all cases the limiting current was due to the total amount of ions present in the gas.

It was shown that the temperature of the electrode surface is ca. 1000 K less than the calculated adiabatic flame temperature and that the maximum flame temperature and maximum ionisation occurred in a stiochiometric flame. It was also shown that the concentration (ion current) of ions in the flame was linearly dependant on the solution used to introduce the ions into the flame.

There is significant absorption of flame borne species into the electrodes inserted into the flame. Which resembles the ion plating/implantation process mentioned in

chapter 1. These flame borne species probably include natural flame species as well as added species. Deposition of gas phase species onto the surface of an electrode inserted into a flame is comparable to a hybrid of the combustion torch method of deposition and the plasma spray method both outlined in section 1.5.

4.0 Electrochemical Diffusion/Junction potential in a gaseous electrolyte

As mentioned in the introduction, when measuring the e.m.f. of an electrochemical cell with different electrode solutions the measured potential difference of the cell includes a junction potential. Using the gas phase electrochemical cell described in this work it is shown that a diffusion potential is also established at the interface between two flowing flame gases containing different concentrations of the same ionic species. The work presented in this chapter has already being published as "Electrochemical diffusion potential in the gas phase", in Electrochemistry Communications, 3, 2001, 675-681.

The cell potential for an electrochemical cell is an additive contribution of the Redox potential and the junction potential, equation (45)

$$(45) \qquad \Delta \Phi_{CELL} = \left[\left(\Phi_{Pt}^R - \Phi^R \right) - \left(\Phi_{Pt}^L - \Phi^L \right) \right] + \left(\Phi^R - \Phi^L \right)$$

where ϕ is the electrical potential for each platinum electrode and gas phase given by the superscripts denoting the left or right cell. The first term on the right of equation 45 describes the Redox potential in a concentration cell and the second part describes the diffusion potential.

The rest of this chapter will show that the measured potential difference in this gas phase electrochemical cell is a consequence of the interface between the two gases.

4.1 Potential difference versus time traces (with different additives)

Potential measurements were made by inserting two similar 1.0 mm diameter platinum wire electrodes into the flame, one in each half and connecting them to an electrometer. The electrodes were positioned 5.0 mm above the burner top plate and 5.0 mm apart. This position was chosen as it is at the tip of the primary reaction zone where the concentration of ions is at a maximum (see figure 4.8). Once in the

flame the end of electrodes melted and formed a spherical ball of diameter ca, 1.5 mm, which can be seen in the thermal image in figure 4.1. Although the surface area of the electrode does not affect the potential difference measured, (potential is an intensive property), care was taken to ensure that both electrodes were as similar as possible; this was to avoid any differences in the flow characteristics of the gases over the surfaces of the electrodes.
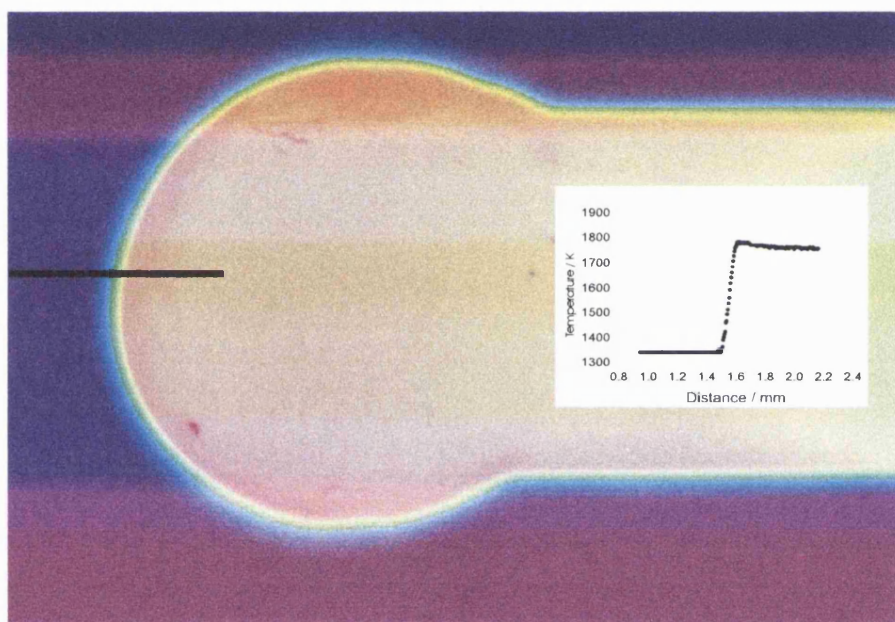
Figure 4.1 A thermal image of a 1.0 mm diameter platinum wire electrode and inset the thermal data associated with the line on the image. Also visible is the spherical bead at the end of the electrode created through melting of the metal on insertion into the flame.

When the two electrodes are positioned in flame B (table 4), one in each side, the potential difference measured between the electrodes is 0.0 V ± 10 mV. The reason we get a 0.0 V reading from this set-up is because when using a Meker burner, we get a laminar flame and any horizontal cross-section through the flame is

homogeneous and isothermal, provided both sides of the flame are identical and so the physical and chemical processes at each electrode surface will be similar and therefore cancel each other out. This is shown in figure 4.2 (a), the potential time transient for the Pt/Pt electrode system in the natural unseeded flames.

When de-ionised water is aspirated into the left hand side flame only, we also see no change in the measured potential difference, figure 4.2 (b). Although H_2O may participate in other neutral flame reactions and may change the equilibrium conditions of many of these reactions it does not effect the concentration of natural flame ions by a measurable amount. Also the introduction of water to one half of the cell does not alter the temperature at the electrode surface measured using an optical pyrometer.

When however a 0.005 M solution of CsCl is aspirated into the left hand side flame we do see a change in the measured potential difference, from 0 to − 0.24 V, figure 4.2 (d). The measured change in the potential difference on the introduction of the CsCl solution was attributed to the increase in total gaseous ion concentration in the left hand side flame relative to the right hand side flame. The increase in ion concentration occurred through ionisation of cesium (IE = 376 kJ mol^{-1})[68] to produce Cs$^+$ and free electrons by the thermal ionisation reaction[69] (11).

Also shown in figure 4.2(c) is the potential time transient for the case where $ZnCl_2$, 0.005 M was added to the left hand side flame. Again we see no change in the measured potential difference. This is because zinc does not ionise under the flame conditions used in this study, (Zn, IE = 906 kJ mol^{-1})[70] so the total ion concentration in the left flame remained unchanged relative to the right flame.

The positive terminal of the electrometer was connected to the left electrode and when the electrometer contacts were swapped the potential difference remained but the polarity was changed.
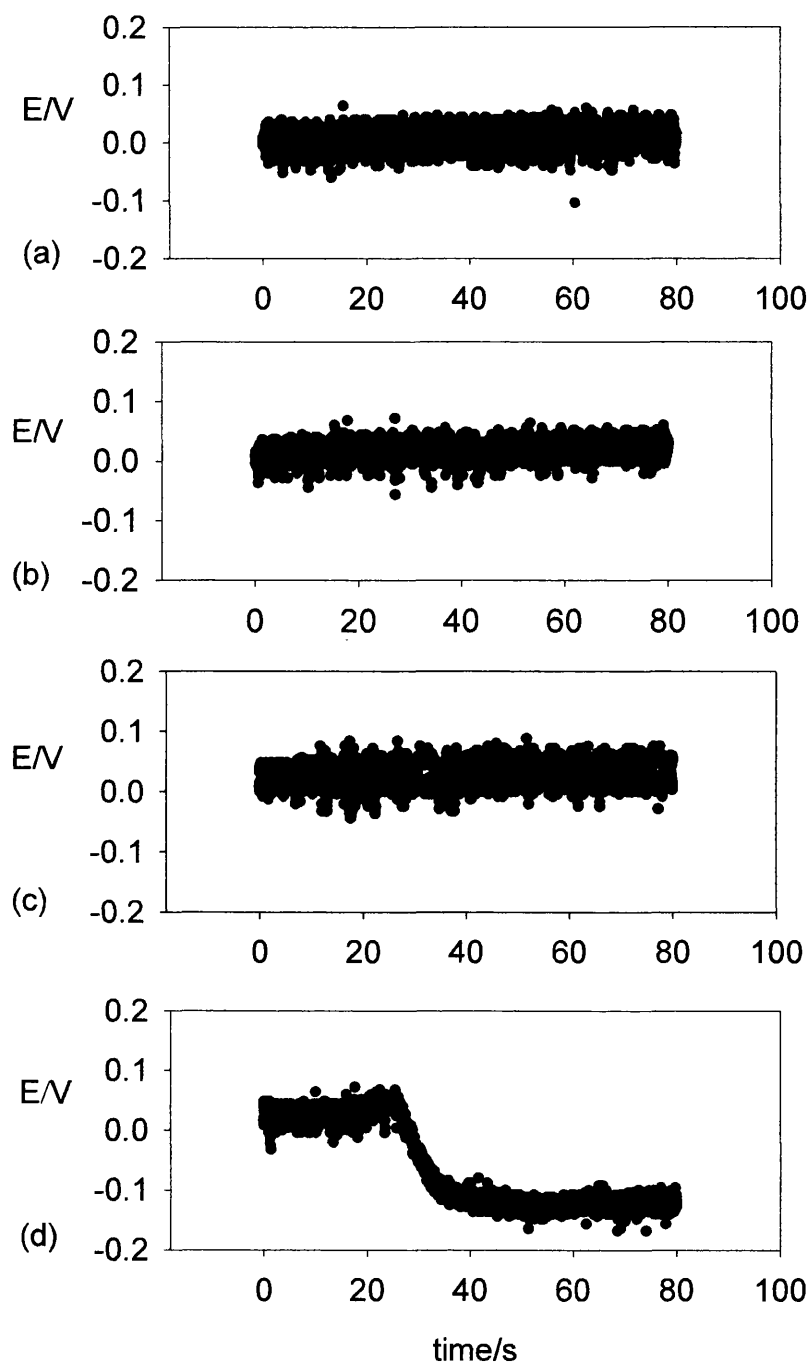
Figure 4.2 Potential time transients for Pt/Pt electrode system in flame B. The unseeded flame (a), with de-ionised water added to the left flame (b), with $ZnCl_2$, 0.005 M added to the left flame (c) and with CsCl 0.005 M added to the left flame (d), the humidifier used to introduce the solutions was switched on at 20 seconds.

This experiment was repeated with aqueous solutions of the chlorides of the Alkali earth metals, Rb, Li, K, and Na and the first row transition metals Zn and Ni. The result is presented in figure 4.3. Changes in the potential difference measured between the two indicator electrodes measured when the alkali metals were introduced into the left side of the flame and no change in potential difference was measured when the transition metals were introduced into the left side of the flame.

.
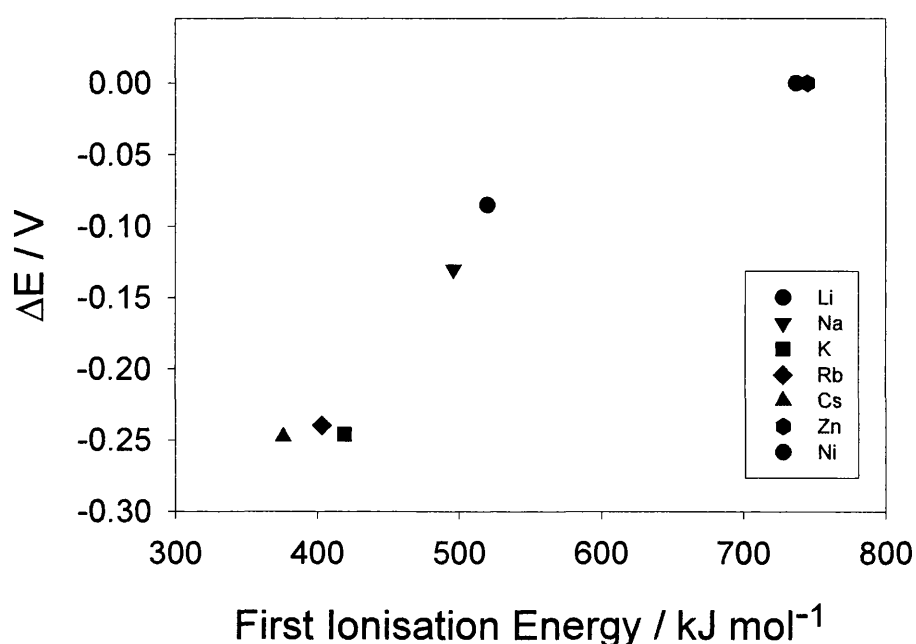
Figure 4.3 The change in potential difference on the introduction of 0.005 M solutions of the group 1 metal chlorides and the chlorides of the transition metals zinc and nickel into the left flame. The positive terminal of the electrometer was connected to the left electrode.

In a fuel rich flame with a burnt gas temperature of 2400 K, the free cesium (IE 396 kJ mol^{-1}) atoms will be 99.6 % ionised according to Goodings and Hayhurst[71], Here when cesium chloride is aspirated into the left side of the flame a potential difference of - 240 mV, versus the natural unseeded flame is recorded. When lithium (IE 520 kJ mol^{-1}) chloride was added to the left flame a potential change of

-80 mV (circle in figure 4.3) was recorded. Zinc (IE 906 kJ mol^{-1}) chloride however did not register a change in potential difference (hexagon in figure 4.3) due to the small amount of ions created from this metal[72].

4.2 Potential difference versus cesium solution concentration

The design of the gas phase electrochemical cell allowed the concentration of solutions being added to the two compartments of the cell to be manipulated independently, this allowed us to alter the relative concentration of ions and electrons present in the two flames. Although the absolute concentration of ions in the flame is not known, we do know that the concentration of ions in the flame is linearly proportional to the concentration of the solution used to aspirate the metal into the flame (see figure 3.7), between the range 0.02 M and 10^{-6} M for cesium chloride. This feature of the apparatus allowed us to control the ratio of ion concentrations between the two compartments of the cell.

An experiment was performed where the concentration of CsCl solution added to the right flame was kept constant at 0.005 M and the concentration of CsCl added to the left flame was varied between 0.02 and 10^{-6} M. The two platinum electrodes were set up as before, 5 mm above the burner and 5.0 mm apart one in each half of the cell. The results from this experiment are presented in figure 4.4. The potential difference measurements were made for 40 seconds and averaged and the error bars are the standard deviation.

The Redox potential contribution to the overall potential in this gas phase cell is likely to be small. This is because the two flames are at equal temperatures and so the equilibrium constants (K) (equation 46) will be equal for both sides of the cell, although the extent of ionisation may be different.

(46) $$K = \frac{[Cs^+][e^-]}{[Cs]}$$

However as Cs has a very low ionisation energy it may be assumed that the extent of ionisation tends toward one ($\to$ 1) and that all of the cesium is ionised in this range of concentrations (see conductivity section). This being the case the electrode
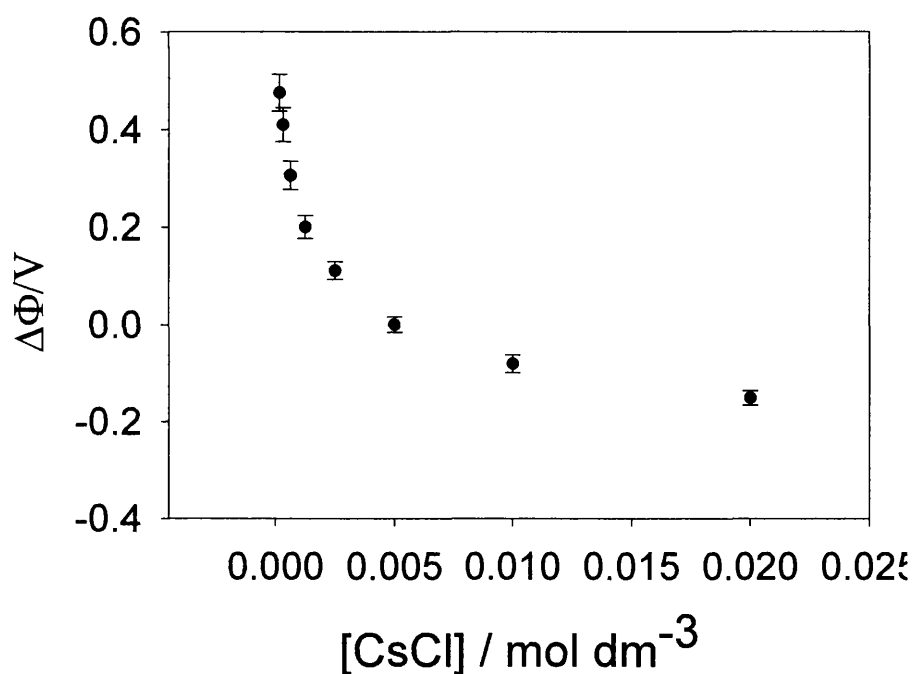
Figure 4.4 Plot of potential difference versus the concentration of CsCl solution introduced into the left hand side flame at 1800 K. A constant 0.005 M solution of CsCl was added to the right hand side flame. The positive terminal of the electrometer was connected to the left electrode.

reactions at both electrodes will be under the same equilibrium conditions thus minimising any redox type potentials.

Diffusion potentials arise due to the differences in mobility's of the charge carriers. Here the difference in mobility's between the charge carriers (cations and electrons)

is vast so the diffusion potential contribution to the total potential is likely to be considerable. The magnitude of the diffusion potential depends on the difference in mobility's of the positive and negative charge carriers, cations and electrons in this case. The mobility of a Cs^+ ion in an atmospheric pressure flame is estimated to be 5.0 cm^2 V^{-1} s^{-1}, which is an average value, obtained from several workers using several different techniques[73]. Similarly the mobility of an electron in an atmospheric pressure flame is estimated[74], to be 4000 cm^2 V^{-1} s^{-1}.

This difference in mobility means that the electrons will diffuse across the junction between the two flames from high to low concentration faster than the Cs^+, even though both are subject to the same concentration gradient[75]. This separation of charge disrupts the electroneutrality at the interface even though the flame remains electroneutral overall. Resulting in the low concentration side having a net negative charge (excess electrons) and the high concentration side having a net positive charge (excess cations). The potential difference that is measured between the two electrodes remains constant because although the flames are flowing the electrode effectively sees a static flame with the charge separation in place.

The junction between the flames forms at the base of the flame in the primary reaction zone, and is sharp. As the flame travels upward (downstream) the junction becomes less defined due to diffusion and turbulent mixing. At any point in the flame however a steady state condition exists where the magnitude of the potential difference and the thickness of the interface remains constant. Further downstream the two phases will be mixed by turbulent flow, resulting in the loss of the interface and thus the potential difference.

A diffusion potential between two electrodes separated by a gas/gas interface, with the two gases having different concentrations of the same species is given by,(47)

(47) $\Delta\Phi_{diffusion} = (\Phi^R - \Phi^L)$

Diffusion potentials have been well studied in the liquid phase and the theory for estimating magnitudes is well developed. The expression for estimating a diffusion potential in an electrochemical cell with the same electrolyte in both compartments but with different concentrations (a type 1 junction)[76] is given by the Henderson equation, equation (48).

$$(48) \quad \Delta\Phi_{diffusion} = \left(\frac{u_+ - u_-}{u_+ + u_-} \right) \frac{RT}{F} \ln\left(\frac{\Sigma a_i^L}{\Sigma a_i^R} \right)$$

where u_+ and u_- are the mobility's of the positively and negatively charged species and a_i^L and a_i^R are the thermodynamic activities of the charged species in the left and right flames. The derivation[77],[78] of equation (48) is based on the following restrictions concerning the diffusion layer (a) the flux across the interface is in steady state, (b) electroneutrality is conserved (c) restriction to one class of mobile cations and one class of mobile anions (i.e. ions of the same charge).

The (gas phase) diffusion potential was estimated by assuming that all ions behave ideally and that only Cs^+ and free electrons were the only charged species present that contribute to the diffusion potential, which satisfies the above assumptions. Figure 4.5 uses the data from figure 4.4 to show the linear plot of potential difference versus the natural logarithm of the ratio of CsCl concentration in both sides of the flame. The solid line in figure 4.5 is the best fit line to the equation (48) using non linear least squares fitting with $Y = (u_+ - u_-/u_+ + u_-)$, as the only fitting parameter, and the temperature to be 1800 K. Y was found to be- 0.903 ± 0.02 (calculated- 0.9975) which is consistent for a system where the anionic charge carriers are more mobile that the cations. The discrepancy between the experimental and calculated results may be an effect of species that were neglected in the calculation i.e. Cl^- ions, which would lower the mean anionic mobility and $Cs^+.H_2O$, which would lower the mean cationic mobility, although not to the same extent.

This result was repeated by Goodings et. al. (reference 73) except their diffusion potential measurement was made vertically along the flame axis using the burner as a base electrode and a metal plate downstream as a working electrode. In order to fit their experimental measurement to equation (48) another term needed to be added to account for the potential drop between the bulk plasma and the working electrode. This is because the two electrodes used in their experiment were not identical, as they were in the experimental set-up used in to make the gas/gas diffusion potential measurements in this project. The added term in equation (49) made allowances for the potential drop in the ion sheath surrounding the working electrode,

$$(49) \qquad \Delta\Phi_{diffusion} = \left(\frac{u_+ - u_-}{u_+ + u_-}\right)\frac{RT}{F}\ln\left(\frac{\Sigma a_i^L}{\Sigma a_i^R}\right) + 0.000674[T_S(O) - T_S(z)]$$
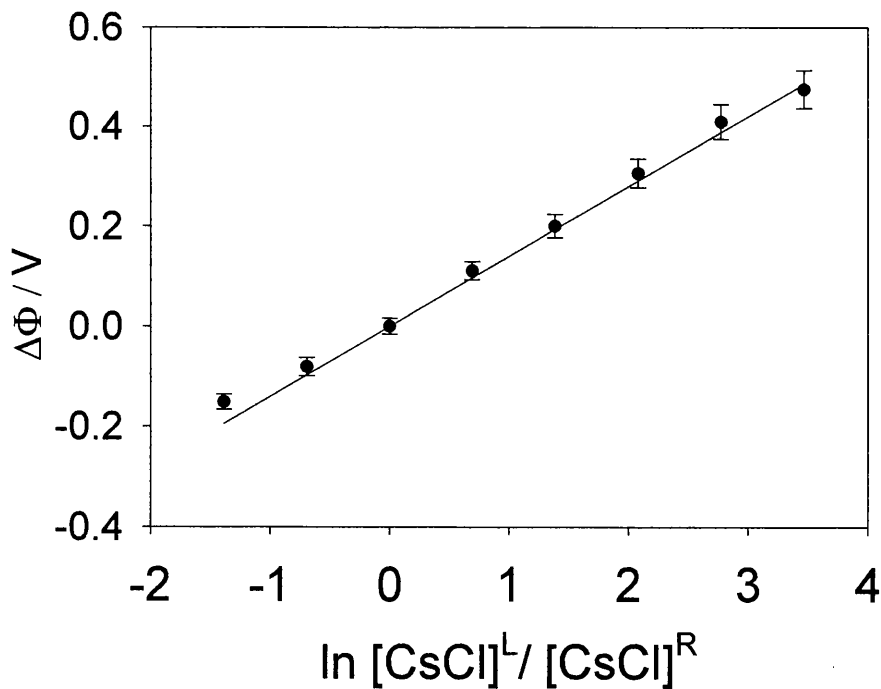

Figure 4.5. Plot of potential difference versus $\ln([CsCl^R/[CsCl]^L)$ for the same data as figure 4.4. The solid line is the best-fit line to Eq. (48).

Where $T_S(O)$ and $T_S(z)$ are the temperatures of the sheath at the base of the flame (O) and some point downstream (z). The constant 0.000674 is found empirically. This theory was tested beautifully by altering the temperature of the water cooled WE by increasing/decreasing the water flow rate, this resulted in predictable changes in the potential difference measured.

4.3 Change in temperature

Analysis of equation (48) shows that the change in the diffusion potential is linearly proportional to the natural log of the changes in the concentration of solution added to the left flame, as all the other terms in the equation are constant. If however we changed the temperature at which the measurements are made, the potential would still be linearly proportional to the natural log of the concentration of solution in the left flame but the gradient of the slope in figure 4.5 would be different for the two different temperatures.

This theory was tested by repeating the diffusion potential experiment above except with the CH_4/O_2 ratio altered in order to change the temperature of the flame while keeping both flames fuel rich and keeping the gas exit velocity constant. In the first experiment the gas flow rates were, O_2 1.6 L min^{-1}, N_2 0.8 L min^{-1}, CH_4 0.8 L min^{-1}, (flame B) with the temperature at the electrode surface measured at 1690 K, and the adiabatic flame temperature calculated to be 2932.4 K. In the second experiment the gas flow rates were, O_2 1.8 L min^{-1}, N_2 0.8 L min^{-1}, CH_4 0.6 L min^{-1}, with the electrode surface temperature measured at 1590 K, and the adiabatic flame temperature calculated to be 2828.4 K, each set up having an equal gas exit velocity, 3.2 L min^{-1}.

The result is shown in figure 4.6. Here the change in the gradient is due to the change in temperature. The difference between the calculated flame temperature and the measured temperature at the electrode surface is due to heat conduction and

radiation by the platinum electrodes. Using the gradient of the slope of the best fit lines in figure 4.6 to calculate the temperature gives, black line 1508 K and red line 1392 K which are approximately 200 K lower than the measured temperatures.
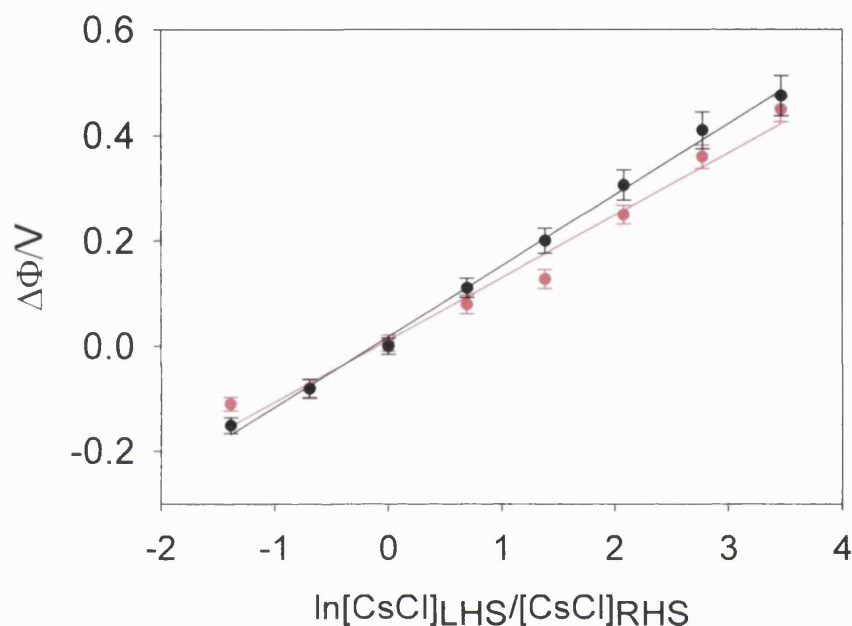
Figure 4.6 Plot of potential difference versus ln ($[CsCl^L/[CsCl]^R$) when the electrode surface temperature was 1690 K (black) and 1590 K (red), as measured with an optical pyrometer (± 20 K) The electrodes were placed 5 mm above the burner and 5.0 mm apart. The flame conditions are stated in the text.

4.4 Total gas exit velocity

Figure 4.7 shows how the potential difference measured between two platinum electrodes in the flame changes with the gas exit velocity. The left hand compartment had 10 mM, CsCl aspirated into it and the right hand side flame had 1.0 mM, CsCl aspirated into it. The gas flow rates were increased while keeping the

ratio O_2 : CH_4 : N_2 constant. The potential difference is independent of the gas flow rate and is only dependent on the concentration gradient and relative mobility's of the charge carriers. Increasing the flow rates of the gases has two effects, one it will push the point of maximum ionisation upward into the flame and secondly it will decrease the degree of turbulent mixing and lateral diffusion at any point on the junction.
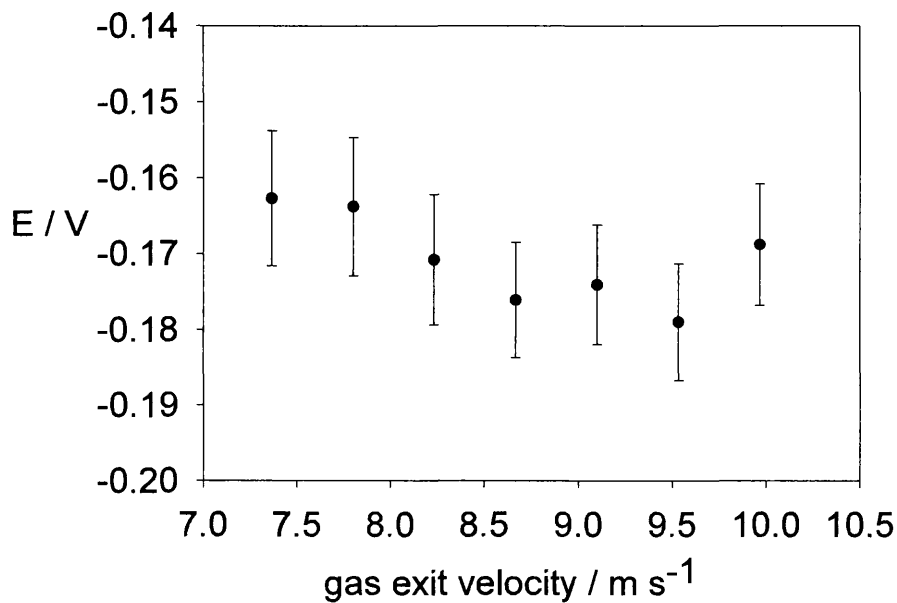
Figure 4.7 Plot of potential difference versus gas exit velocity with a constant 10 mM CsCl added to the left side and 1 mM CsCl added to the right side. The electrodes were placed 5 mm above the burner and 5 mm apart.

4.5 Concentration profile of ions in the vertical direction

The concentration of ions in the vertical axis of the flame is not uniform and has its maximum at approximately 5 mm above the burner plate, which is just at the tip of the primary reaction zone. Figure 4.8 shows the potential difference measured between two Pt electrodes as a function of height above the burner. The electrodes were placed 5.0 mm apart (one in each compartment) in the same horizontal plane and raised from 1.25 mm above the burner surface to 27.25 mm above the burner

surface. The electrodes themselves were 1.0 mm diameter and so the spatial resolution of the plot is low, of the order of one electrode diameter. 10 mM of CsCl was added to the RHS of the cell and 1 mM of CsCl was added to the LHS of the cell.
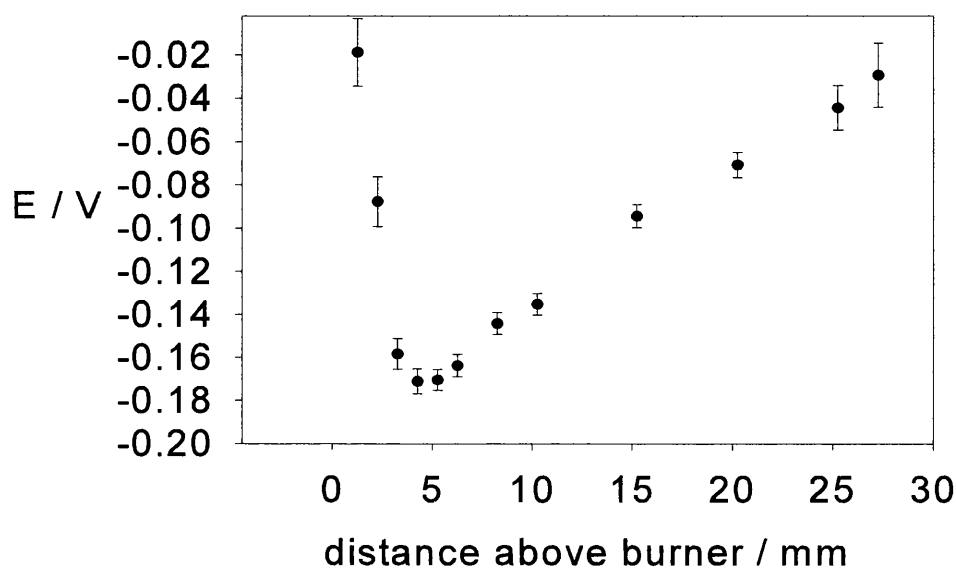
Figure 4.8 This plot shows how the potential difference and thus the ion concentration change as a function of height above the burner in the vertical direction. Here a constant 10 mM CsCl was added to the left side and 1 mM CsCl was added to the right side. The electrodes were placed 5.0 mm apart and the potential difference measured at different heights above the burner surface.

When the potential is converted to concentration using the Henderson equation (equation 48), we can see that the concentration of Cs^+ in the vertical axis will have its maximum just above the PRZ, approximately 5 mm above the burner surface, see figure 4.9. The ions then exponentially decay, where at ca. 25 mm above the

burner surface the difference in ion concentration between the two compartments is undetectable. This result is in good agreement with Mass Spectroscopic studies[79].
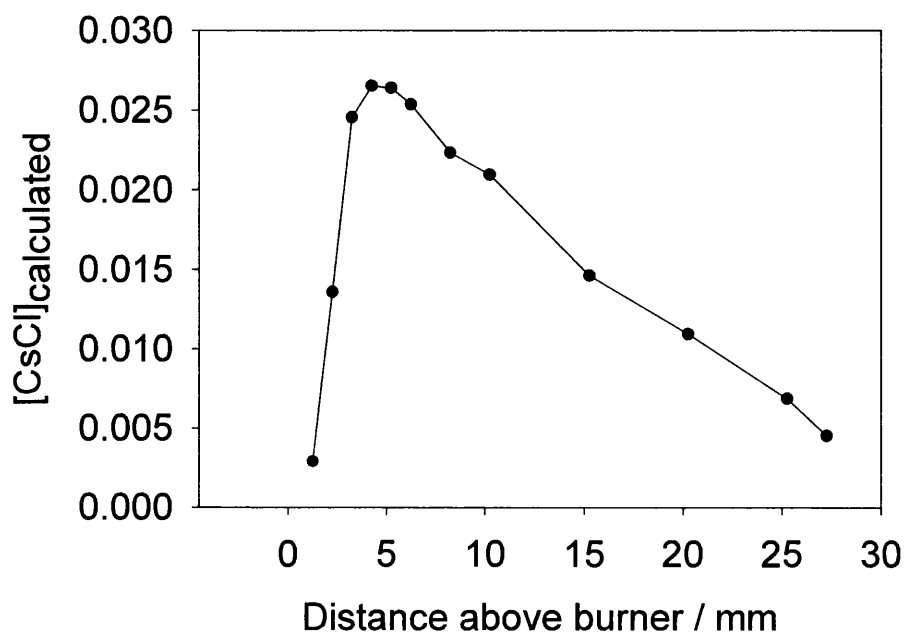
Figure 4.9 Shows the same data as figure 4.8 but with the potential difference converted to concentration using equation (48).

4.6 Conclusions

The measurement of an electrochemical potential difference between two metal electrodes in a gas phase electrochemical cell is described. Using a specially designed dual burner where the concentration of ions could be manipulated, a concentration gradient between the two flames was established and a potential difference was measured. The potential difference was dependent only on the presence and concentration of ions in the flame, and so it is concluded that the potential difference is electrochemical in nature. This potential difference that

develops between the two flowing flames with different concentrations of charge carriers (ions and free electrons) was analysed using theory developed for junction potentials in the liquid phase. This is the first time such theory has being applied to the gas phase. This theory describes the relationship between concentration of ions, ion mobility's and potential difference for charge carriers in the liquid phase and the agreement is good for the gas phase. The potential difference was also found to be temperature dependant and independent of gas flow rate. A different approach has being employed by Goodings[80] to measure diffusion potentials in the gas phase. Here a diffusion potential was measured in the vertical direction between the burner (upstream) and a metal plate (downstream) and a similar expression for the diffusion potential derived in terms of the concentration gradient.

The potential difference measured here was dependant on the presence and the concentration of ions in the flame and so it is concluded that the basis of the potential difference is electrochemical. Other physical effects may contribute to the potential difference like soret thermal diffusion and Seebeck effects[81] but as the magnitude of the potential differences being measured here are of the order of 100's of mV coupled with no measurable temperature difference between the electrodes these contributions will be small.

5.0   Evidence for electrochemical redox potentials in the gas phase.

In chapter 4, the measurement and characterisation of diffusion potentials at the gas/gas interface between two flowing flames was described. Here the same experimental technique is employed to measure the potential difference due to electrochemical redox potentials, for different ionised chemical species in the gas phase. The work presented in this chapter has already being published as "Electrochemical redox potential in flame plasma", in Electrochemistry Communications, 4, 2002, 780-786.

This was achieved by making concurrent ion current and potential difference measurement between the two indicator electrodes, using the electrode set-up shown schematically in figure 5.1.
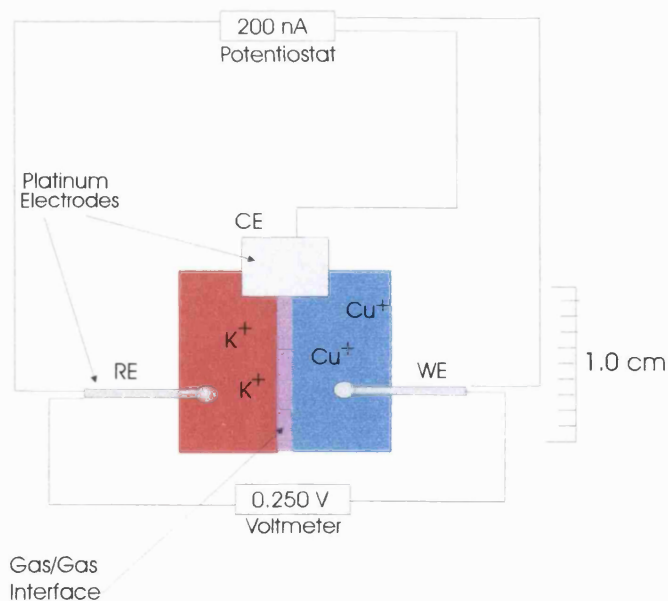

Figure 5.1 Schematic diagram of the electrode set-up used to make the concurrent ion current and potential difference measurements in the gas phase cell.

The ion current was measured for both electrodes and the potential between them measured while the concentration of additive introduced into the working compartment was varied. The reason concurrent measurements were made was that different species would ionise to different extents, see figure 4.3, and in order to make comparisons between different species, the concentration (ion current) and potential difference generated needed to be measured over a range of different solution concentrations. Then comparisons of the potential differences at a particular ion concentration could be made for different species. A schematic of the electrode set up used to make these measurements is shown in figure 5.1. The aim was to maintain one flame at a constant concentration of ionisable additive whilst changing the concentration of additive on the other side. Essentially the cell is analogous to an electrochemical cell with transference until the concentration of the charged species in both flames is equal, then the diffusion potential contribution to the total potential difference is insignificant and the potential difference measured is due only to the redox potentials of the gas phase ions.

5.1   The cell reaction

When potassium chloride and copper chloride solutions for example, are added to the two halves of the flame respectively the cell may be represented as in (50), for clarity only the metal atoms and atomic ions are considered.

(50) $Pt \mid K_{(g)}, K^+_{(g)} : Cu^+_{(g)}, Cu_{(g)} \mid Pt'$
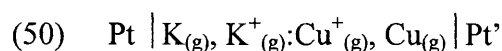
With the total cell reaction being (51)

(51) $K_{(g)} + Cu^+_{(g)} = K^+_{(g)} + Cu_{(g)}$
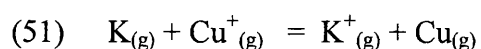
The Nernst equation for this reaction is (52).

$$(52) \quad E = E^{\theta} + \frac{RT}{nF} \ln \frac{a_{Cu^+} a_K}{a_{K^+} a_{Cu}}$$

5.1.1 Formulation of a gas phase cell potential

The total cell potential for the above cell is given by, (53)

(53)

$$\Delta\phi_{cell} = \Delta\phi_{redox} + \Delta\phi_{diffusion} = [(\phi^{Pt'} - \phi^g_{Cu/Cu^+}) - (\phi^{Pt} - \phi^g_{K/K^+})] + (\phi_{Cu/Cu^+} - \phi_{K/K^+})$$

The total cell reaction may be written, (54)

$$(54) \quad K_{(g)} + Cu^+_{(g)} + e^-_{(Pt')} = K^+_{(g)} + Cu_{(g)} + e^-_{(Pt)}$$
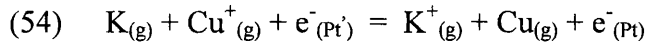
This reaction is only true for the ionised species that are in equilibrium near the surface of the platinum indicator electrodes and that the electrons originate form the electrodes[82],[83]. If these conditions are meet then we can write, (55)

$$(55) \quad \overline{\mu}_i^g = \overline{\mu}_i^{Pt}$$

Where $\overline{\mu}_i^g$ and $\overline{\mu}_i^{Pt}$ are the electrochemical potential of each species in the gas phase and metal respectively for only one electrode. This can be expanded to take both electrodes and all species, so at equilibrium, (56)

$$(56) \quad \overline{\mu}_{K^+}^g + \overline{\mu}_{Cu}^g + \overline{\mu}_{e^-}^{Pt'} = \overline{\mu}_K^g + \overline{\mu}_{Cu^+}^g + \overline{\mu}_{e^-}^{Pt}$$

Where $\overline{\mu}_M^g$ is the electrochemical potential of each species. We can calculate the electrochemical potential for each species from[84], (57)

(57) $\bar{\mu}^g_{M^+} = \mu^{\circ g} + zF\phi + RT \ln a^g_{M^+}$

Where the $\mu^{\circ g}$ is the chemical potential for the ion under standard conditions (atmospheric pressure and 298 K), ϕ is the electrical potential of the flame plasma, and $a^g_{M^+}$ is the activity for that species. Equation (56) can be expanded using equation (57) and rearranged to give equation (58).

(58)

$$(\bar{\mu}^{(Pt)}_{e^-} - \bar{\mu}^{(Pt')}_{e^-}) = (\bar{\mu}^{\circ g}_{Cu^+} + \bar{\mu}^{\circ g}_{K} - \bar{\mu}^{\circ g}_{K^+} - \bar{\mu}^{\circ g}_{Cu}) + RT \ln\left(\frac{a^g_{Cu^+} a^g_K}{a^g_{K^+} a^g_{Cu}}\right) + \left(zF\phi_{Cu/Cu^+} - zF\phi_{K/K^+}\right)$$

The term on the right side of equation (58) is the cell potential, $\Delta\Phi_{cell}$. The first term on the left side of equation (58) is related to the standard electrode potential for the cell, E°_{rctn}, which can be given by (59),

(59) $-nFE^{\circ}_{rctn} = \bar{\mu}^{\circ g}_{Cu^+} + \bar{\mu}^{\circ g}_{K} - \bar{\mu}^{\circ g}_{K^+} - \bar{\mu}^{\circ g}_{Cu} = \Delta G^I_{Cu/Cu^+} - \Delta G^I_{K/K^+}$

where $\Delta G^I_{Cu/Cu^+}$ and $\Delta G^I_{K/K^+}$ are the free energy of ionisation of the gaseous metal to give the metal ion. The last term in equation (58) is the diffusion potential term already discussed in chapter 4.

Calculation of $\Delta G^I_{Cu/Cu^+}$ and $\Delta G^I_{K/K^+}$ from $\Delta H_{Ionisation}$ and $\Delta S_{Ionisation}$ data will give the potential difference expected for this cell when only the atomic ions are present, as is discussed in section 5.6. Any variation from this value can be attributed to the presence of other ions that may be present, e.g. CuH_2O^+.

5.2 The electrode set-up for concurrent conductivity and potential measurements

A three electrode system was used to make the conductivity measurements. The electrodes consisted of two Platinum wire electrodes, 1mm in diameter, which were inserted into the flame cell one in each compartment, 5 mm above the burner and 5 mm apart. These wire electrodes were used as the Working Electrode (WE) and the Reference Electrode (RE), depending on which compartment was being analysed. The third, Counter Electrode (CE), was a Platinum flag (1 cm^2) which was placed 1 cm downstream of the other two electrodes, equidistant from both. The ion current measurements were made with a potentiostat (μAutolab II, Eco chemie B.V.), by measuring the maximum ion current at $- 5$ V, versus the other platinum wire electrode in the opposite compartment. The measurements were taken three times and averaged. Flame B was used for this experiment.

The potential difference measurements were made between the RE and WE mentioned above and were recorded using an in house built buffer amplifier (100 MΩ input impedance) in conjunction with a digital storage oscilloscope (Tektronix, TDS 3012). The measurements were taken for 40 seconds at 100 Hz and averaged. The standard deviation was taken as the error, which was typically $\pm$ 10 mV.

5.3 The change in ion current versus changes in the concentration

The cation current was measured using Langmuir type probes[85], which give a characteristic cyclic voltammagram (figure 1.7). The current generated at $- 5$ V in a flame seeded with KCl (0.05 mM), in the reference compartment of the cell was measured and found to be 250 nA. The cation current generated in the flame in the working compartment was then measured with a range, of different concentrations of KCl solutions added to the flame gases. The cation current was found to be

proportional to the concentration of the metal salt solution used to introduce the metal ions into the flame, as was discussed earlier in chapter 3.

5.4   The change in potential difference versus changes in the concentration

The potential difference was measured between the two platinum electrodes placed in the two compartments of the cell. The left-hand side (LHS) compartment of the cell was used as a reference half-cell. Where the flame was seeded with a constant concentration of additive (0.05 mM KCl), and the right hand side (RHS) compartment was used as a variable working half-cell, seeded with different concentrations of KCl ranging from 0.1 mM to 0.03 mM. Here changing the concentration of the solution used to introduce the metal ions into the flame alters the concentration of ions present in the flame. The potential difference measured between the two electrodes was found to be proportional to the concentration of the solution used to introduce the metal ions into the RHS flame. This was discussed in chapter 4 and shown graphically in figure 4.5.

5.5   The potential difference versus ion concentration for different species

Figure 5.2 shows the potential difference's measured when potassium chloride, copper chloride and magnesium chloride, respectively, are added to the working half cell while potassium chloride is being added to the reference half cell. Here the x-axis is the ratio of the ion concentration on the RHS to the LHS. So when the concentration of ions on both sides is equal, a ratio of 1, the diffusion part of the total potential difference is predicted to disappear, according to equation 5.14. This being the case the remaining potential difference will be due to differences in the electrochemical redox potentials of the ions present in the different compartments of the cell.
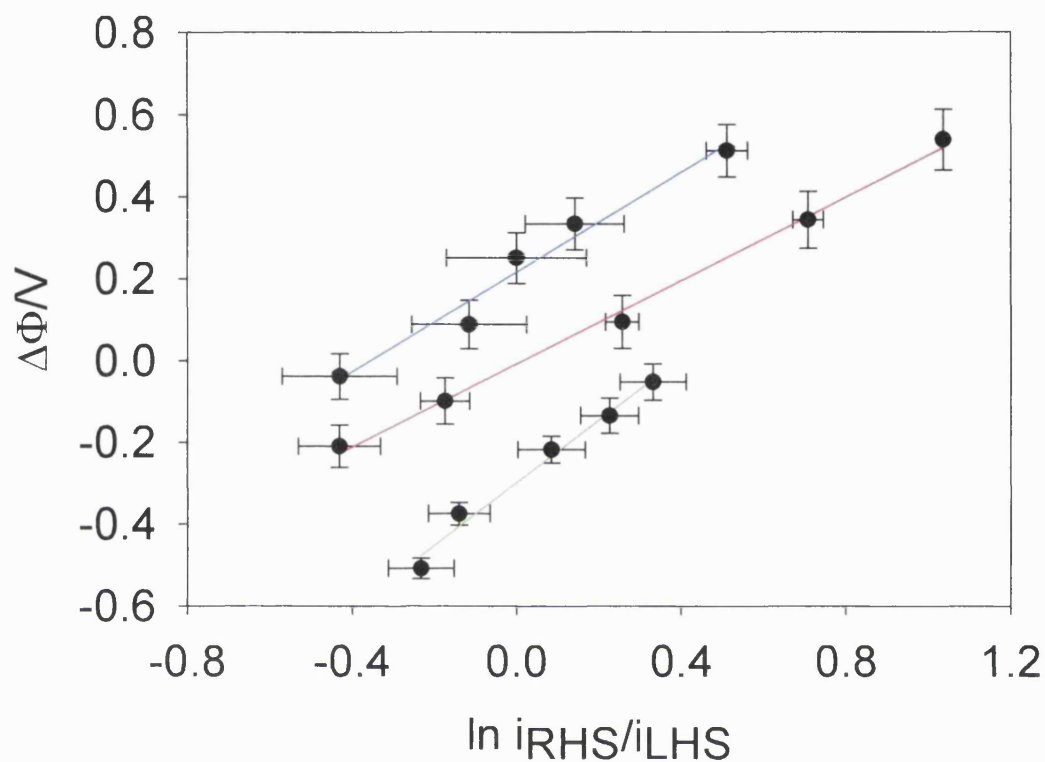
Figure 5.2 The potential differences measured versus the ratio of ion currents for the right and left flames. A 0.05 mM solution was added to the LHS and was kept constant. CuCl$_2$ (green), KCl (red) and MgCl$_2$ (blue) were then added to the RHS from stock solutions of 10.0, 0.1 and 2.0 mM respectively.

When CuCl$_2$ was added to the RHS flame and KCl was added to the LHS flame and the ion concentrations on both sides were equal, as measured amperometrically, a potential difference of - 0.280 V was measured between the two platinum electrodes. When MgCl$_2$ was added to the RHS again with KCl added to the LHS, a potential difference of + 0.240 V was measured between the electrodes. When KCl was added to the RHS compartment and again KCl was added to the LHS of the cell, the potential difference measured, at the equivalence point, was 0.0 V ± 10

mV. The gradients for the best-fit line for the copper/potassium and magnesium/potassium cells in figure 5.2 are higher than the gradient for the potassium/potassium cell, due to the presence of redox potential. The magnitude of the potential difference in the K/K cell above fitted well with the Henderson equation (48) for diffusion potentials as was discussed in section 4.

Equation (60) means that if we know the zero current cell potential, E_{cell} at a specified composition then we can calculate the reaction Gibbs energy at that composition and vice versa.

(60) $-nFE_{cell} = \Delta_r G$

Calculation of the reaction standard Gibbs energy, $\Delta_r G^{\theta}$, (61) for the gas phase reaction allows us to compare the standard cell potential, E^{θ} (62) and the measured cell potential, E_{cell}.

(61) $\Delta_r G^{\ominus} = \Delta G^{I}_{A^+/A} - \Delta G^{I}_{B^+/B}$

(62) $-nFE^{\theta}_{cell} = \Delta_r G^{\theta}$

So for the above cells Cu^+/K^+ and Mg^+/K^+, the standard electrode potentials are calculated to be, - 3.38 V and + 0.09 V respectively which compare with the measured values of $-$ 0.28 V and + 0.24 V, obtained from the gas phase cell.

The potential differences measured here, when the diffusion potential contribution had been eliminated from the cell by equating the concentration of ions in both compartments, are dependant on the identity of the metal chloride added to the flame. Thus it is concluded that the physical basis of these potential differences is due to the thermodynamic activities of the various ionic species.

5.6 The potential differences measured for different species versus a natural flame.

A similar experiment was also performed, again using flame B, in which the LHS flame was not seeded with any additive and the RHS flame was seeded with various concentrations of metal chlorides. The cation current data generated here was then plotted against the potential difference data measured versus the natural unseeded flame in the reference compartment. An arbitrary value of 100 nA was chosen for the cation current, the potential differences measured between the electrodes for the different species, when the cation currents were equal to this value, were then compared and are shown in table 5. Also shown in table 5 are the major ions found in flames seeded with these particular metal salts, taken from mass spectroscopic measurements from various sources, the data for the group 1 metals are from Butler and Hayhurst[86].

Table 5. Potential differences generated from different metal chlorides added to RHS of the flame cell versus the reference half of the cell, an unseeded flame, using flame B. The potential measurement was made when the ion current at -5 V are equal to -100 nA in the RHS flame. Also shown are the major ions present that will contribute to the potential difference.

Species	Caesium	Potassium	Sodium	Lithium	Calcium[87]	Magnesium[88]
ΔE vs. natural flame	-0.320	-0.120	-0.185	-0.040	-0.115	-0.081
Major ions present	Cs^+ $CsOH_2^+$	K^+ KOH_2^+	Na^+ $NaOH_2^+$	Li^+ $LiOH_2^+$	$CaOH^+$ Ca^+ $Ca(OH)_2H^+$ $CaOH_2^+$	Mg^+ $MgOH_2^+$ $Mg(OH)_2H^+$ $MgOH^+$

The electrochemical cell potential differences E_{cell} measured here are an additive contribution of the diffusion potential and the redox potentials according to (63)

$$(63) \quad E_{cell} = \Delta\phi_{redox} + \Delta\phi_{diffusion} = [(\phi^{Pt'} - \phi^g_{Cu/Cu^+}) - (\phi^{Pt} - \phi^g_{K/K^+})] + (\phi_{Cu/Cu^+} - \phi_{K/K^+})$$

The thermodynamic activities and the mobility's for all the ionised species in the cell can be related through (64)

$$(64) \quad E_{CELL} = E^0_{reaction} + \frac{RT}{F}\ln\left(\frac{a^R_{Cu^+}a^L_K}{a^L_{K^+}a^R_{Cu}}\right) + \left(\frac{u_+ - u_-}{u_+ + u_-}\right)\frac{RT}{F}\ln\left(\frac{\Sigma a^L_i}{\Sigma a^R_i}\right)$$

As discussed in the introduction the assumption is that all the ionic species behave ideally, $\gamma_\pm = 1$, so the activity terms can be replaced by concentrations. As the concentration of ions was equal from cell to cell, it is clear to see that the cell potential measurement E_{cell} contains contributions from a redox potential source and from a diffusion potential source. The diffusion potential contribution will have a constant value from cell to cell because it is concentration dependent, but the redox part of the total potential will vary from species to species.

5.7   Conclusions

Redox potentials of gas phase ions have being measured in the presence of and in the absence of diffusion or junction potentials. The potential determining processes were related to the ionisation of metal chlorides added to the flame and are dependent on the identity of the metal chloride. The interpretation of the electrochemical cells is discussed in relation to two possible cell configurations, which differ on the basis of the electrode composition. As we have seen in chapter 3, the electrodes can absorb some of the gas phase species present in the flame thus forming an amalgam type of electrode. In this case the cell may be represented as (65)

(65)   Pt, K | K$^+$$_{(g)}$: Cu$^+$$_{(g)}$, | Cu, Pt'
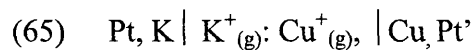
With the cell reaction being writing as (66)

(66)   K$_{(s)}$ + Cu$^+$$_{(g)}$ = K$^+$$_{(g)}$ + Cu$_{(s)}$
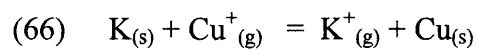
With the Nernst equation being (67)

(67) $E = E^{\theta} + \dfrac{RT}{nF} \ln \dfrac{a_{Cu^+}}{a_{K^+}}$

The difference between this cell representation and the cell representation in section 5.1 is that, in latter arrangement the activity of the reduced metal will be unity (solid). Most probably the cell reaction is a combination of these two interpretations.

6.0   Conclusions

This thesis presents significant steps toward the establishment of electrochemical methodology using a gaseous electrolyte. The electrochemical measurements made include diffusion potentials at the gas/gas interface, which were found to be dependant on the ion concentration gradient between the two gases. Electrochemical redox potentials of ions in a gaseous electrolyte were also measured. This was achieved by combining potentiometric and amperometric measurements. The amperometric measurements ensured that the concentration of ions was equal in both halves of the gas phase electrochemical cell this eliminated the diffusion potential. The potential difference measured between the half-cells, containing different species, when the concentrations of ions were equal was assigned as the redox potential of the gaseous ions.

The controlled electroreduction of gas phase metal ions was also investigated. And it was concluded that the application of dynamic electrochemistry methodology to ions in the gas phase was found not possible using this flame system. Attempts were made to resolve reduction or oxidation waves using various metals as reference electrode (sacrificial Mo and inert Pt) and examining for several different gas phase ionic species. But in all cases the limiting current was due to the total amount of ions present in the gas.

The concentration of ions in a flame can be altered measurable, by aspirating solutions of ionisable metal salts of known concentration, into the flame.

The ion concentration in the flame is linearly proportional to the concentration of aqueous salt solution used to introduce the ions into the flame, over the approximate range 0.1M to 1.0 μM, of salt solution.

A special burner design has allowed the study of the gas/gas interface, by controlling the concentration gradient of ions between the two gases.

The potential difference measured between two platinum electrodes inserted one in each half of the flame cell was dependant on the ion concentration gradient between the two gases.

The potential determining process is related to the ionisation potential of the gas phase ions.

The Henderson equation (3.3), derived for liquid phase electrochemistry also describes the relationship between concentration of ions, ion mobility and potential difference measured in the gas phase.

By equating the concentration of ions on either side of the gas/gas interface, the diffusion potential contribution to the total cell potential could be eliminated. This allowed the measurement of redox potentials of the gas phase ions, by comparing different species in the different compartments.

References

1   A von Engle, *Electric Plasmas, their nature and uses*, Taylor and Francis Ltd., London, 1983.

2   Jamal Ghoroghchian, Fereshteh Sarfarazi, Timothy Dibble, John Cassidy, Jerry J. Smith, Andrea Russel, Gordon Dunmore,Martin Fleischmann, Stanley Pons, *Electrochemistry in the gas phase*, Anal. Chem., 1986, **58**, 2278.

3   Yun Fang, Johan Leddy, *Voltammetry in gas phase environments*, Journal of Electroanalytical Chemistry, 1995, **384**, 5.

4   J. M. Googings, J. Guo, A. Hayhurst, S. Taylor, *Current-voltage characteristics in a flame plasma: analysis for positive and negative ions, with applications*, International Journal of Mass Spectrometry, 2001, **206**, 137.

5   J.Janek, C.Rosenkranz *Plasma-Electrochemical Growth of AgBr Layery on AgCl Substrates*, J. Phys. Chem. B 1997, **101**, 5909.

6   M. Vennekamp, J. Janek, *Plasma electrochemical growth of ion-conducting AgBr and AgCl*, Solid State Ionics, 2001, **141-142**, 71.

7   Z. Ogumi, Y. Uchimoto and Z. Takehara, *Electrochemistry using Plasma*, Advanced Materials, 1995, **3**, 7.

8   S.D.T.Axford, J.M.Goodings, A.N.Hayhurst, *Mass-Spectroscopic Sampling of Ions from Flames at Atmospheric Pressure*, Combustion and Flame, 1998, **114**, 294.

9   S.T.D. Axford, A.N. Hayhurst, *Int. J. Mass Spec., Ion Process*, 1991, **110**, 31.

10 J. Lawton, F. J. Weinberg, Eds., D. Bradley, *Electrical Aspects of Combustion*, Clarendon Press, Oxford, 1969, p.215.

11 A. G. Gaydon, H. G. Wolfhard,, *Flames, Their Structure, Radiation and Temperature*, Halsted Press 1979, p.340.

12   Q. Tran. N. S. Karellas, J. M. Goodings, *Ion Chemistry of the Transition Metals in Hydrocarbon Flames 1 & 2*, Can. J. Chem., 1988, **66**, 2210.

13   S.D.T.Axford, J.M.Goodings, A.N.Hayhurst, *Mass-Spectroscopic Sampling of Ions from Flames at Atmospheric Pressure,* Combustion and Flame, 1998, **114**, 294.

14   P. R. Smy and A. Ibn. Noor, *High-pressure Langmuir probe in a weak flowing plasma or plasma sheath,* Journal of Applied Physics, 1976, **47**, 1327.

15   Alexander B. Fialkov, *Invesstigations of Ions in flames*, Prog. Energy Combust. Sci.,, 1997, **23**, 399.

16   Carl J. Butler, Allen N. Hayhurst, *Reactions of H_3O^+ ions with free atoms of copper and with molecules of CuOH in gaseous flames,* J. Chem. Soc., Faraday Trans., 1997, **93**, 1497.

17   Carl J. Butler and Allen N, Hayhurst, *Kinetics of gas-phase ionisation of an alkali metal, by electron and proton transfer reactions in fuel rich flames at 1800-2250 K,* J. Chem. Soc., Faraday Trans., 1998, **94**, 2729.

18   W.J.Miller, *Ions in flames*, The Combustion Institute, 14th Symposium on Combustion, 1973, p.312.

19   Axford S. D. T., Hayhurst A. N., J. Chem. Soc. Faraday Trans., 1995, **91**, 827.

20   Hayhurst A. N., Telford N. R., J. Chem. Soc., Faraday Trans. 1, 1974, **70** 1999.

21   Hayhurst A. N., Telford N. R., J. Chem. Soc., Faraday Trans. 1, 1975, **71** 1352.

22   Alexander B. Fialkov, *Invesstigations of Ions in flames*, Prog. Energy Combust. Sci.,, 1997, **23**, 453.

23   P. F. Knewstubb, T. M. Sugden, *Mass-Spectroscopic Studies of Ionisation in Flames. I. The Spectrometer and its applications to ionisation in Hydrogen*

Flames, Proceedings of the royal society of London, May 10, 1960, **255**, 520.

24   A. G. Gaydon, H. G. Wolfhard,, *Flames, Their Structure, Radiation and Temperature,* Halsted Press 1979, p.355.

25   John M. Dyke, Properties of Gas Phase Ions, J. Chem. Soc., Faraday Trans. 2, 1987, **83**, 69

26   J.Warnatz, U.Maas, R.W.Dibble, Ed., *Combustion,* Springer, 1996, p. 74.

27   A. G. Gaydon, H. G. Wolfhard, *Flames,* 4th Edition, Wiley, Chapman and Hall, 1979, p. 357.

28   Carl J. Butler and Allen N, Hayhurst, *Kinetics of gas-phase ionisation of an alkali metal, by electron and proton transfer reactions in fuel rich flames at 1800-2250 K,* J. Chem. Soc., Faraday Trans., 1998, **94**, 2729.

29   A. F. Ashton and A. N. Hayhurst, *Kinetics of Collisional Ionisation of Alkali Metal Atoms and Recombination of Electrons with Alkali Metal Ions in Flames,* Combustion and Flame, 1973, **21**, 69.

30   A. N. Hayhurst, N. R. Telford, Trans. Faraday Soc., 1970, **66**, 2784.

31   Carl J. Butler, Allen N. Hayhurst, *Reactions of H_3O^+ ions with free atoms of copper ane with molecules of CuOH in gaseous flames,* J. Chem. Soc., Faraday Trans., 1997, **93**, 1497.

32   A. G. Gaydon, H. G. Wolfhard, *Flames, Their structure, radiation and temperature,* 4th edition, Chapman and Hall, London, 1979, p. 340.

33   A. M. Shaw, J. M. Dyke, A study of the chemiionization reactions of Ca, Sr and Ba with $O_2(X^3\Sigma_g\text{-})$, Chemical Physics, 1994, **179**, 455

34   Q. Tran, N. S. Karellas, J. M. Goodings, *Ion Chemistry of the Transition Metals in Hydrocarbon Flames,* 1 & 2, Can. J. Chem., 1988, **66**, 2210.

35   Q. Tran, N. S. Karellas, J. M. Goodings, *Ion Chemistry of the Transition Metals in Hydrocarbon Flames,* 1 & 2, Can. J. Chem., 1988, **66**, 2210.

36   Ashok K. Vijh, *Electrode potentials and interface plasmons in the metal/gaseous electrolyte interphasic region,* Materials Chemistry and Physics, 1986, **14**, 47.

37   R.G.Compton, G.H.W.Sanders, *Electrode Potentials,* Oxford Chemistry Primers, p. 69.

38   Maher I Boulqis, Piere Fauchais, Emil Plender, *Thermal Plasmas: Fundamentals and Applications,* Vol 1, 1994.

39   A von Engle, *Electric Plasmas, their nature and uses,* Taylor and Francis Ltd., London, 1983.

40   Allen J. Bard, Larry R. Faulkner, *Electrochemical Methods, Fundamentals and Applications,* John Wiley and Sons, 1980, p.510.

41   P.W.Atkins, *Physical Chemistry, 4th Ed.* Oxford, p.25.

42   B. Earl, L. D. R. Wilford, Chemistry Data Book, Nelson Blakie, 1992

43   P.W.Atkins, *Physical Chemistry,* 4th Ed. Oxford, p.963.

44   CRC Handbook of Chemistry and Physis, 57th Ed., CRC Press, 1976-77, F-62.

45   CRC Handbook of Chemistry and Physis, 57th Ed., CRC Press, 1976-77, E-59.

46   F. L. Tufts, Phys. Rev., 1906, **22**, 193.

47   Langmuir, I., Gen. Elec. Rev., 1924, **27**, 449.

48   A. G. Gaydon, H. G. Wolfhard, *Flames, Their Structure, Radiation and Temperature,* Halsted Press, 1979, p.340.

47   W.J.Miller, *Ions in flames,* The Combustion Institute, 14th Symposium on Combustion, 1973, p.312.

50   S.D.T.Axford, J.M.Goodings, A.N.Hayhurst, *Mass-Spectroscopic Sampling of Ions from Flames at Atmospheric Pressure,* Combustion and Flame, 1998, **114**, 294.

51   P. W. Atkins, *The elements of Physical Chemistry 2n Ed.* Oxford University Press, 1996, p. 23.

50   M.Vennekamp, J.Janek, *Plasma electrochemical growth of ion conducting AgBr and AgCl,* Solid State Ionics, 2000, **141-142**, 71.

53   R. Cescotti, *Burners and flame technology,* Journal of the Institute of fuel, 1968, **77**, 77.

54   R. M. Fristrom, *Flame Structure and Processes*, Oxford University Pres, New York, 1995.

55   Ashok K. Vijh, *Electrode potentials and interface plasmons in the metal/gaseous electrolyte interphasic region,* Materials Chemistry and Physics, 1986, **14**, 47.

56   Sean P. McCormack, *Master of Chemical Research Thesis,* University College London, U.K., September 2000.

57   Carl J. Butler, Allen N. Hayhurst, *Reactions of H_3O^+ ions with free atoms of copper and with molecules of CuOH insigaseous flames,* J. Chem. Soc., Faraday Trans., 1997, **93**, 1497.

58   P. R. Smy and A. Ibn. Noor, *High-pressure Langmuir probe in a weak flowing plasma or plasma sheath,* Journal of Applied Physics, 1976, **47**, 1327.

59   D. Bradley, S. M. A. Ibrahim, *Determination of positive ion mobilities and collision cross sections in flame gases using electrostatic probes*, J. Phys. D: Appl. Phys, 1974, **7**, 1377.

60   N. R. Telford, *Computer Program, according to the method of A.G.Gordon.* Cambridge University in 1969.

61   A.G. Gaydon and H.G. Wolfhard, *Flames : their structure, radiation and temperature,* London :Chapman and Hall, 1979.

62   J.Warnatz, U.Maas, R.W.Dibble, Ed., *Combustion,* Springer, 1996, p. 43.

63   A. C. Fisher, *Electrode Dynamics,* Oxford Chemistry Primers 34, Oxford Science Publications, 1996.

64   J. Lawton, F. J. Winberg, Eds. D. Bradley *in Electrical aspects of combustion,* Clarendon Press, Oxford, 1969 p.162.

65 J. D. Vyas, K. L. Choy, *Structral characterisation of thermal barrier coatings deposited using electrostatic spray assisted vapour deposition method,* Materials Science and Engineering A, 2000, **277**, 206.

66 N. J. Archer, *The Plasma assisted Chemical Vapour Deposition OF TiC, TiN and TiC$_X$N$_{1-X}$,* Thin Solid Films, 1981, **80**, 221.

67 S. Hogmark, P. Hollman, A. Alahelisten, P. Hedenqvist, *Direct Current Bias applied to hot flame diamond deposition produces smooth low friction coatings,* Wear, 1996, **200**, 225.

68 CRC Handbook of Chemistry and Physis, 57th Ed., CRC Press, 1976-77, F-62.

69 A. F. Ashton A. N. Hayhurst, *Kinetics of Collisional Ionisation of Alkali Metal Atoms and Recombination of Electrons with Alkali Metal Ions in Flames,* Combustion and Flame, 1973, **21**, 69.

70 CRC Handbook of Chemistry and Physis, 57th Ed., CRC Press, 1976-77, F-62.

71 S.D.T.Axford, J.M.Goodings, A.N.Hayhurst, *Mass-Spectroscopic Sampling of Ions from Flames at Atmospheric Pressure,* Combustion and Flame, 1998, **114**, 294.

72 Q. Tran. N. S. Karellas, J. M. Goodings, *Ion Chemistry of the Transition Metals in Hydrocarbon Flames 1 & 2,* Can. J. Chem., 1988, **66**, 2210.

73 Alexander B. Fialkov, *Investigations on Ions in Flames,* Prog. Energy Combust. Sci., 1997, **23**, 399.

74 Alexander B. Fialkov, *Investigations on Ions in Flames,* Prog. Energy Combust. Sci., 1997, **23**, 399.

75 A von Engle, *Electric Plasmas their nature and uses,* Taylor and Francis, London and New York, 1983.

76 A. J. Bard, L. R. Faulkner, *Electrochemical Methods,* John Wiley and Sons New York, 1980, p. 63.

[77] W.E. Morf, *Calculations of Liquid- Junction Potentials and Membrane Potentials on the Basis on the Planck Theory*, Analytical Chemistry, 1977, **49**, 810.

[78] John M. Goodings, Jingzhong Guo, James G. Laframboise, *Electrochemical diffusion potential in a flame plasma, theory and experiment*, Electrochemistry Communications, 2002, **4**, 363.

[79] Christine C.Y.Chow, John M. Goodings, *Ion chemistry of second row transition metals in hydrocarbon flames: cations and anions of Y, Zr, Nb, and Mo*, Can. J. Chem., 1995, **73**, 2263.

[80] John M. Goodings, Jingzhong Guo, James G. Laframboise, *Electrochemical diffusion potential in a flame plasma, theory and experiment.* Electrochemistry Communications, 2002, **4**, 363.

[81] D. M. Rowe, *CRC Handbook of Thermoelectrics*, CRC Press, 1995, p. 2.

[82] A. J. Bard, L. R. Faulkner, *Electrochemical Methods Fundamentals and applications,* John Wiley and Sons, 1980, p. 61.

[83] Ashok K. Vijh, *Electrode Potentials and Interface Plasmons in the metal/gaseous Electrolyte (i.e. plasma) Interphasic Region.* Materials Chemistry and Physics, 1986, **14**, 47.

[84] D. R. Crow, *Principals and applications of electrochemistry, fourth edition,* Blackie Academic, 1994, p. 93.

[85] A.G. Gaydon, H.G. Wolfhard, *Flames, Their structure, radiation and temperature, 4ed,* Chapman and Hall, London, 1979 p. 340.

[86] Carl J. Butler, Allen N. Hayhurst, J. Chem. Soc. Faraday Trans., 1998, **94**, 2729.

[87] A. M. Shaw, J. M. Dyke, *A study of the chemiionisation reactions of Ca, Sr and Ba with O_2 $(X^3\Sigma_g-)$,* Chemical Physics, 1994, **179**, 455.

[88] QingFeng Chen, Rebecca K. Milburn, Alan C. Hopkinson, Diethard K. Bohme, John M. Goodings, *Magnesium chemistry in the gas phase:*

calculated thermodynamic properties and experimental ion chemistry in H$_2$-O$_2$-N$_2$ flames. International Journal of Mass Spectrometry, 1999, **184**, 153.